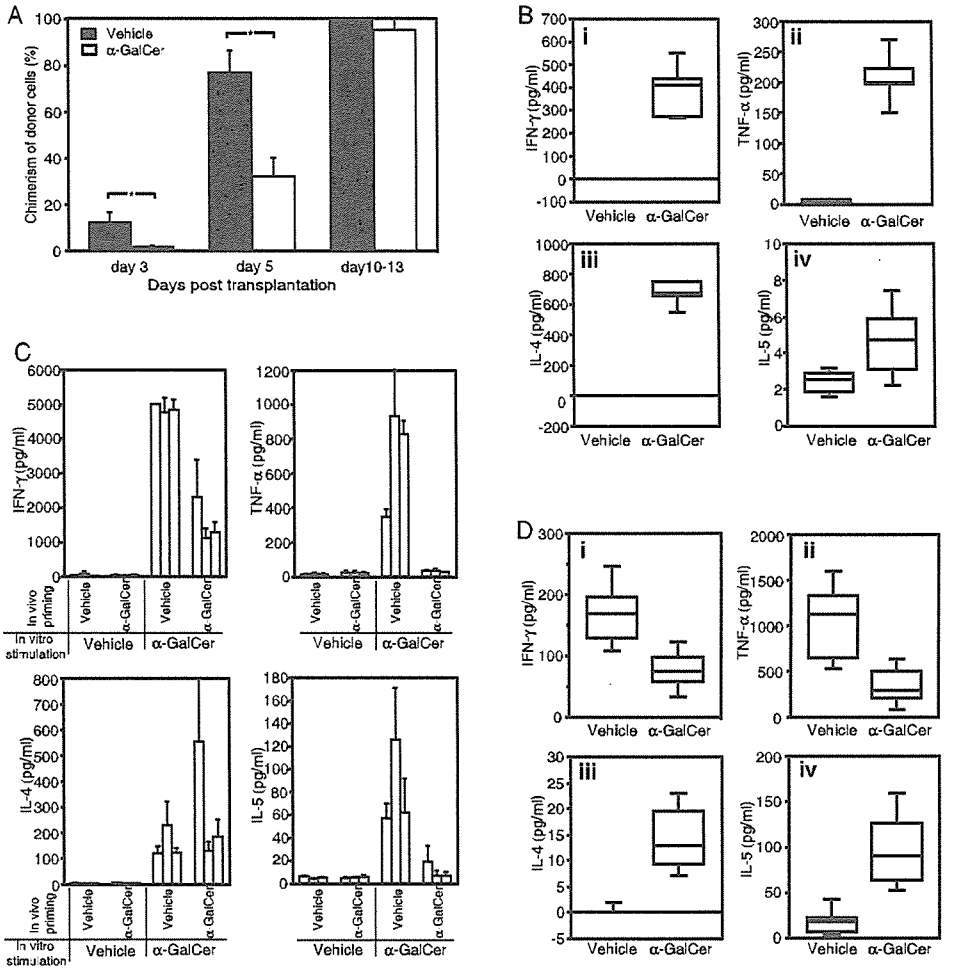

FIGURE 2. $CD4^+$ splenocyte chimerism and serum cytokines of α-GalCer-treated mice. *A*, Chimerism of $CD4^+$ splenocytes in α-GalCer and vehicle-treated recipients. We analyzed $CD4^+$ splenocytes from 6 vehicle- and 6 α-GalCer-treated recipients on day 3, 9 vehicle- and 11 α-GalCer-treated recipients on day 5, and 8 vehicle- and 8 α-GalCer-treated recipients on days 10–13 (median, 11 days). There is a statistically significant difference between the proportions of $CD4^+$ splenocytes from vehicle- and α-GalCer-treated recipients on day 3 ($p = 0.002$) and day 5 ($p < 0.0001$) posttransplant ($p < 0.0001$). *B*, Composite box plots for serum IFN-γ, TNF-α, IL-4, and IL-5 levels in α-GalCer-treated ($n = 6$) or vehicle-treated ($n = 6$) recipients at 3 h after transplantation. The plots for IFN-γ and IL-4 of vehicle-treated mice overlap with zero lines. There are statistically significant differences between the vehicle- and α-GalCer-treated groups with each cytokine (IFN-γ, TNF-α, IL-4 ($p = 0.004$), and IL-5 ($p = 0.037$)). *C*, Cytokine production from in vivo-primed and in vitro-stimulated (6 days after priming) splenocytes by α-GalCer or vehicle. Each group included three mice (each bar indicated the result from one mouse). Results are the means and SD of triplicate values. *D*, Composite box plots for serum IFN-γ, TNF-α, IL-4, and IL-5 levels in α-GalCer-treated ($n = 16$) or vehicle-treated ($n = 14$) recipients on day 5 or 6 posttransplant. There are statistically significant differences between the vehicle- and α-GalCer-treated groups with each cytokine ($p < 0.0001$). Serum from the individual mice was used to measure all four cytokines (*B–D*).

Host-residual iNKT cells are required for the prolongation of survival by adoptively transferred iNKT cells

The above observations suggest that adoptively transferred iNKT cells attenuate GVHD by affecting host-residual iNKT cells. To examine the different roles of host-residual and transferred iNKT cells more clearly, we used $J\alpha18^{-/-}$ (iNKT cell-deficient) BALB/c and C57BL/6 mice as hosts and donors, respectively.

We compared the survival time between $J\alpha18^{-/-}$ and wild-type BALB/c mice after transplantation from wild-type C57BL/6. When $J\alpha18^{-/-}$ BALB/c mice were used as recipients, the survival of these mice was significantly shorter than that of wild-type BALB/c mice after transplantation ($p = 0.017$, Fig. 4*A*). Importantly, the prolongation of survival by either the adoptive transfer of iNKT cells (Fig. 4*B*) or the administration of α-GalCer (data not shown) was not observed if the recipients were $J\alpha18^{-/-}$ BALB/c mice. Difference in the time course by α-GalCer treatment of donor $CD4^+$ T cell chimerism and the serum cytokine levels at both early phase (3–6 h) and late phase (5–6 days) posttransplant, which was seen when wild-type BALB/c mice were used as the recipients (Fig. 2, *A* and *B*), was not evident when $J\alpha18^{-/-}$ BALB/c mice were the recipients (data not shown). Surprisingly, iNKT cell administration to $J\alpha18^{-/-}$ recipient mice also did not change the levels of IFN-γ, TNF-α, IL-4, and IL-5 at 3–6 h after transplantation (Fig. 4*C*), suggesting that cytokines released after adoptive iNKT administration were produced from host-residual iNKT cells, not from infused iNKT cells.

In contrast, when $J\alpha18^{-/-}$ C57BL/6 mice were used as donors utilizing the same protocol as in the experiment shown in Fig. 1*A* (2 μg of α-GalCer or control vehicle every 4 days from the day of transplantation), the survival of the recipient BALB/c mice was prolonged by α-GalCer administration compared with vehicle administration (Fig. 4*D*), as was survival when wild-type C57BL/6 mice were used as donors (Fig. 1*A*). In this setting (donor: $J\alpha18^{-/-}$ C57BL/6), serum cytokine levels at 3–6 h posttransplant

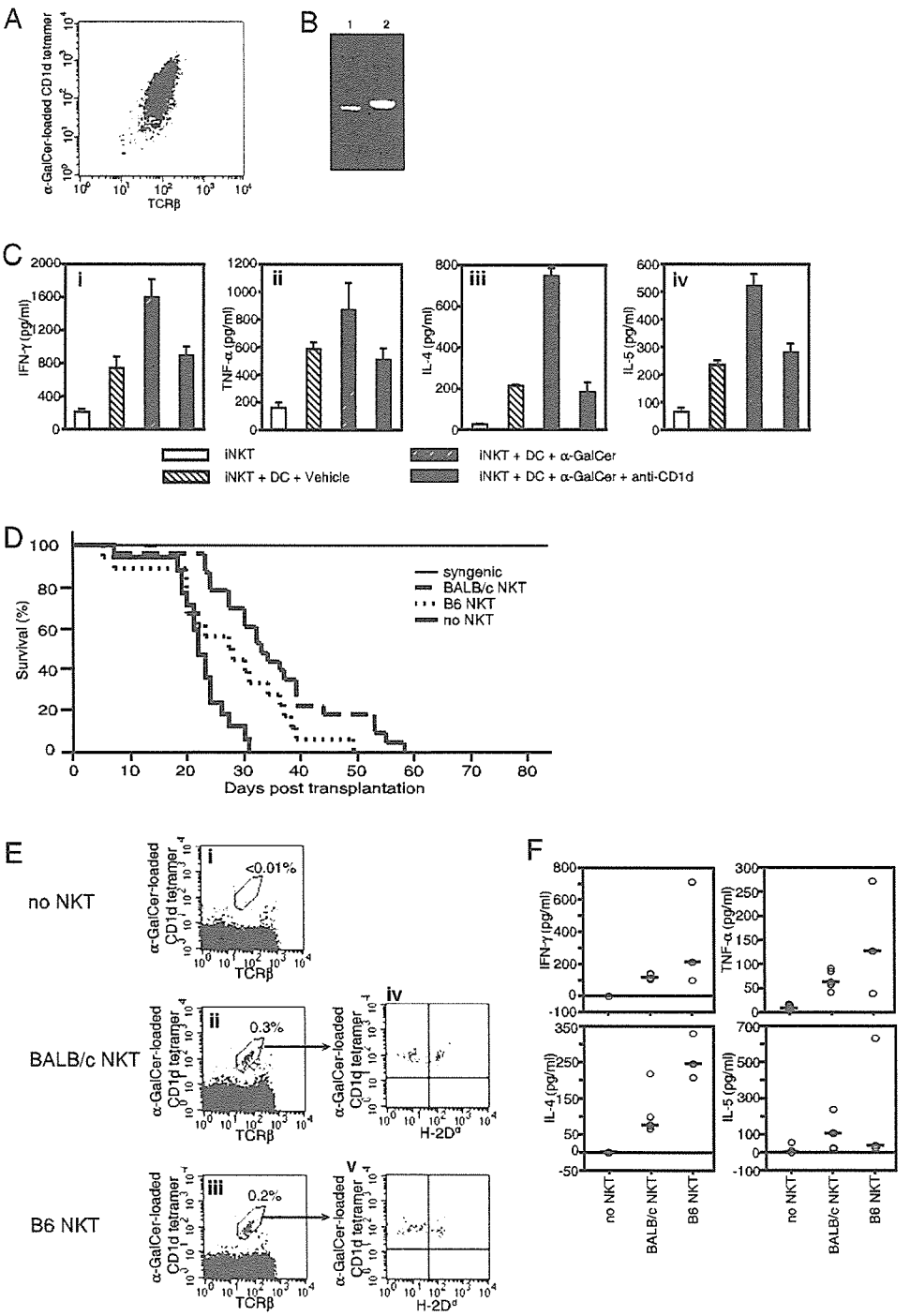

FIGURE 3. Adoptive transfer of in vitro-expanded iNKT cells. *A*, Flow cytometric analysis of in vitro-expanded iNKT cells. α-GalCer-loaded CD1d tetramer and TCRβ double-positive cells indicated iNKT cells. The purity of double-positive cells was 98%. *B*, Electrophoresed PCR products from in vitro-expanded iNKT cells using Vα14-specific 5′ primer and Cα-specific 3′ primer (*lane 1*) and those using β-actin-specific primers (*lane 2*). *C*, Assay for in vitro cytokine production from expanded iNKT cells stimulated by autologous splenic dendritic cells. *D*, Survival of in vitro-expanded iNKT cell-transferred recipients. Recipients receiving both C57BL/6-derived (B6 NKT, $n = 18$) and BALB/c-derived (BALB/c NKT, $n = 23$) iNKT cells survived longer than recipients without iNKT transfer (no NKT, $n = 17$) (C57BL/6-derived iNKT and no iNKT, $p = 0.016$; BALB/c-derived iNKT and no iNKT, $p < 0.0001$). The fine line represents the survival of syngeneic cell-transplanted mice (syngeneic, $n = 7$). *E*, iNKT cells in liver lymphocytes on day 6 posttransplant. α-GalCer-loaded CD1d tetramer and TCRβ double-positive cells in the liver from recipients without iNKT cell transfer (no NKT, *i*) and with the transfer of iNKT cells derived from BALB/c (BALB/c NKT, *ii*), and C57BL/6 (B6 NKT, *iii*) are shown in *left panels*. The origin of iNKT cells was evaluated by staining H-2D^d and α-GalCer-loaded CD1d tetramer (*iv* and *v*). We repeated the evaluation of liver iNKT cells seven times on day 5, 6, or 7 posttransplant. The chimerism of donor/recipient iNKT cells was not affected by the difference in the strain from which adoptively transferred iNKT cells were derived: the average difference between the two groups was as low as 8.6%, with a SD of 2.9% (range, −6 to 12%). *F*, Plots for serum IFN-γ, TNF-α, IL-4, and IL-5 levels at 3 h after transplantation from recipients without iNKT cell transfer ($n = 6$) and with the transfer of iNKT cells derived from BALB/c ($n = 5$) and C57BL/6 ($n = 3$). Horizontal lines indicate the median value. There are statistically significant differences between the "no NKT" and "BALB/c NKT" and "no NKT" and "B6 NKT" groups with each cytokine (no NKT and BALB/c NKT, $p = 0.003$ (IFN-γ, TNF-α, and IL-4) and $p = 0.008$ (IL-5); no NKT and B6 NKT, $p = 0.014$ (IFN-γ, TNF-α, and IL-4) and $p = 0.041$ (IL-5)).

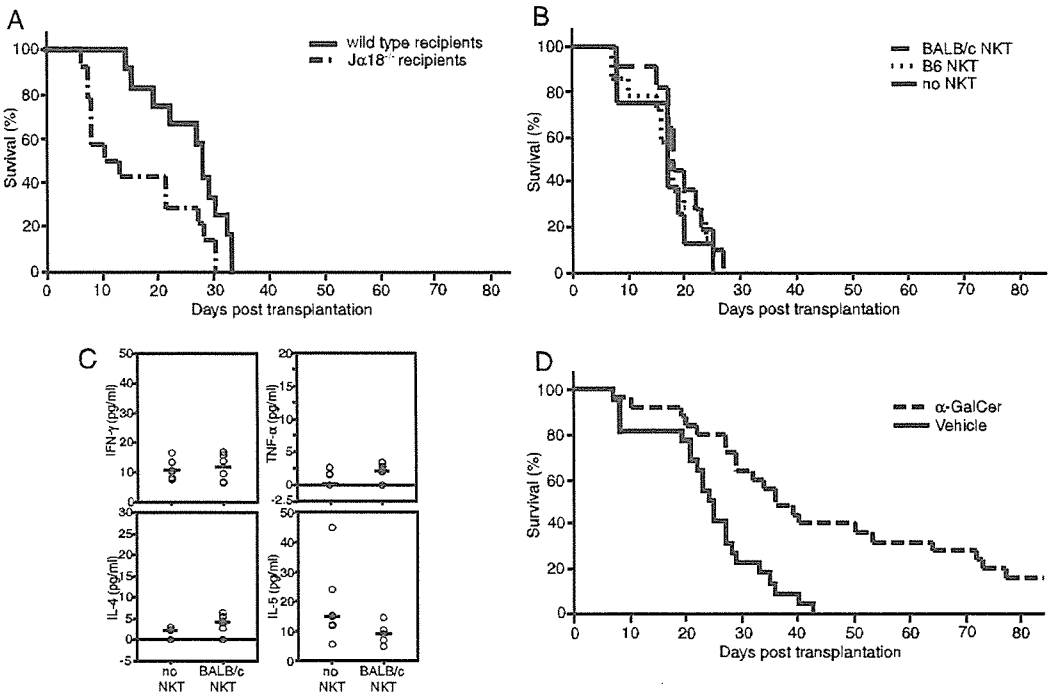

FIGURE 4. Impact of $J\alpha18^{-/-}$ mice on posttransplant survival. *A*, Wild-type ($n = 14$) recipients survived significantly longer than $J\alpha18^{-/-}$ recipients ($n = 12$) ($p = 0.017$). *B*, There was no significant difference among the survival of mice transferred with C57BL/6-derived (B6 NKT, dotted line, $n = 13$)- and BALB/c-derived (BALB/c NKT, $n = 14$) iNKT cells and without iNKT cell transfer (no NKT, $n = 9$). *C*, Plots for serum IFN-γ, TNF-α, IL-4, and IL-5 levels at 3 h after transplantation from $Ja18^{-/-}$ mice transferred with BALB/c derived ($n = 5$) or those without iNKT cell transfer ($n = 5$). Horizontal lines indicate median. *D*, Survival of α-GalCer (dashed line, $n = 25$)- and vehicle ($n = 22$)-treated mice that were transplanted with $J\alpha18^{-/-}$ donor cells. α-GalCer-treated mice survived longer than vehicle-treated mice ($p = 0.002$).

were significantly increased by α-GalCer treatment, and the serum IL-4 and IL-5 levels on 5 or 6 days posttransplant in α-GalCer-treated recipients were higher than those in vehicle-treated recipients and similar to those in wild-type recipients (data not shown).

These results collectively indicated that host-residual iNKT cells, rather than iNKT cells contained in the graft, are the major producers of various Th1 and Th2 cytokines shortly after transplant and key regulators of GVHD, and indeed are required for the regulation of GVHD by graft-contained and -adopted iNKT cells.

Combination of α-GalCer pretreatment and use of iNKT cell-depleted grafts resulted in maximal GVHD reduction and graft rejection

In experiments in which $J\alpha18^{-/-}$ C57BL/6 mice were donors, we noticed that 2 of 25 recipients treated with α-GalCer survived for >100 days, which was not the case if the wild-type C57BL/6 mice were donors (data not shown). Although this could represent a variation in the experimental conditions because there was no significant difference between the two groups, we expected that survival could be maximally improved if host-residual iNKT cells were stimulated before and after transplantation and iNKT cells were absent from the grafts. When we administered α-GalCer on days −4, 0, and 4 of transplantation and transplanted the grafts from $J\alpha18^{-/-}$ C57BL/6 mice, 8 of 17 wild-type BALB/c recipient mice survived for >100 days without obvious GVHD (Fig. 5, *A* and *B*) as expected. Without α-GalCer, there was no obvious difference in the survival of the recipients due to selection of the donor, i.e., wild-type or $J\alpha18^{-/-}$ C57BL/6 mice (cf Fig. 1*A* vs Fig. 5*A* and Fig. 1*B* vs Fig. 5*B*).

Among the eight long-term survivors described above in the setting of $J\alpha18^{-/-}$ C57BL/6 mice as donors and α-GalCer started before transplantation, seven mice completely rejected the donor cells and the remaining one mouse exhibited mixed chimerism at 6 wk posttransplant (data not shown). Therefore, we examined the time course of donor cell chimerism early after transplantation in recipients with α-GalCer that was started before transplantation. Both $Gr\text{-}1^+$ and $CD4^+$ T cells were engrafted in vehicle-treated mice (Fig. 5*C*). In contrast, both $Gr\text{-}1^+$ and $CD4^+$ T cells were rejected early after transplantation in α-GalCer-treated mice. Particularly, $Gr\text{-}1^+$ cells were never engrafted (Fig. 5*C*).

Since it is known that NK cells are major effectors in graft rejection (27) and play a role as effectors of iNKT cells in antitumor immunity by secreting IFN-γ (1, 9), we performed in vivo NK depletion by administering anti-asialo GM1 Ab. It is of note that iNKT was not depleted by this treatment (data not shown). However, the prolongation of survival (Fig. 6*A*) and graft rejection (Fig. 6*B*) by α-GalCer were still observed as seen without anti-asialo GM1 Ab. For graft rejection, therefore, some targets other than NK cells should be considered as effectors of host-residual iNKT cells activated by α-GalCer, particularly in the absence of donor iNKT cells.

Discussion

Many studies have suggested that an important physiological function of iNKT cells is to control immune responses against autoimmunity, infection, and tumors (1, 9). In transplantation immunity, iNKT cells are also thought to play a role in the induction of allograft (28–30) or xenograft tolerance (31). In this study, we examined the role of iNKT cells in GVHD mouse model systems, using an iNKT stimulator α-GalCer, adoptive transfer of in vitro-expanded iNKT cells, and $J\alpha18^{-/-}$ mice (16), and found that host-residual iNKT cells can attenuate GVHD.

Some reports have suggested that both donor bone marrow-derived (10) and host-residual (11, 12) NKT cells ($NK1.1^+$ or $DX5^+$

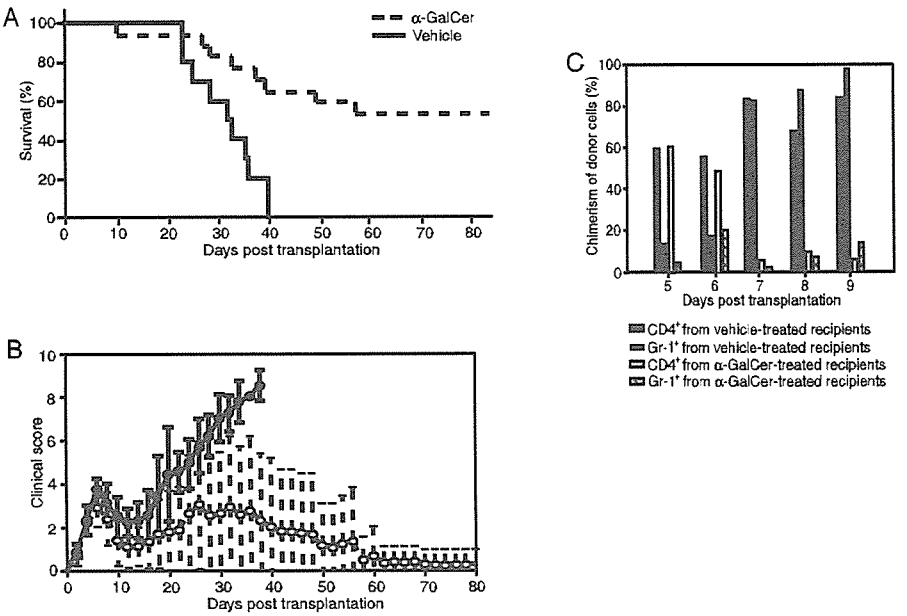

FIGURE 5. Maximal survival accompanied by graft rejection. Treatment with α-GalCer on days −4, 0, and 4 of transplantation. Survival (*A*) and clinical score (*B*, means and SD) of α-GalCer (n = 17)- and vehicle (n = 10)-treated mice that were transplanted with Jα18$^{-/-}$ donor cells. α-GalCer-treated mice lived longer (p = 0.0008). The GVHD score within the first 30 days after transplantation was significantly lower in the α-GalCer-treated group (p < 0.0001). Although the eight mice that survived for >100 days showed few signs of GVHD, they did show graft rejection or long-term mixed chimerism. *C*, Engraftment of CD4$^+$ splenocytes and Gr-1$^+$ bone marrow cells in α-GalCer- and vehicle-treated mice that were transplanted with Jα18$^{-/-}$ donor cells. The representative results of three independent and highly reproducible experiments are shown.

T cells) may suppress acute GVHD. These NKT cell populations should overlap with the iNKT cell population that we describe here. Therefore, the attenuation of GVHD by adoptive transfer of in vitro-expanded iNKT cells described here is consistent with previous results.

Recently, a report has shown that α-GalCer administration to recipients prolonged survival of GVHD mice and its administration to CD1d$^{-/-}$ mice did not prolong their survival (14). Our results show more direct evidence that such findings are caused by the functional activation of iNKT cells, with the use of Jα18$^{-/-}$ mice. Moreover, the need for host-residual iNKT cells was clearly shown by the result that adoptive iNKT cells from either strain did not attenuate GVHD if transferred to Jα18$^{-/-}$ BALB/c recipients.

Surprisingly, host-residual iNKT cells were maintained in the liver early after transplantation if C57BL/6 (donor strain)-derived iNKT cells were transferred, whereas very few host-residual iNKT cells were detected without adoptive iNKT transfer (Fig. 3*C*, *i*, *iii*, and *iv*). We could not distinguish the origin of H-2D^{d+} iNKT cells detected in the recipient liver if BALB/c strain-derived iNKT cells were transferred (Fig. 3*C*, *ii* and *iv*). It is possible that they also represent host-residual rather than injected iNKT cells. Taken together, these findings suggest that the attenuation of GVHD by adoptively transferred iNKT cells is likely to occur through the maintenance of host-residual iNKT cells, although the precise mechanism remains to be elucidated. It should also be clarified whether injected and host-residual iNKT cells locally interact with each other in a specific tissue. Particularly, it would be highly desirable if we could visualize iNKT cells in the liver by marking their strain and origin, which would be possible only after technical advances are available for the specific staining of iNKT cells. Analyzing a direct interaction of liver-isolated iNKT cells and activated MHC-mismatched iNKT cells would be of great interest, but impracticable, given the extremely low proportion of liver iNKT cells. In addition, the α-GalCer-loaded CD1d tetramer is the only tool for specifically staining iNKT cells, and the isolation procedure for iNKT cells might stimulate them and thus influence the results of in vitro analyses.

Other unexpected results include the delay in engraftment, the induction of mixed chimerism, and graft rejection by host-residual iNKT cells, particularly if α-GalCer administration was started before transplantation and Jα18$^{-/-}$ C57BL/6 mice were used as donors. This setting conferred the maximal survival benefit to the recipients because of the mildness of GVHD, albeit this occurred in our meticulous experimental mouse model. Possibly, the activated host-residual iNKT cells may suppress donor CD4$^+$ T cell function or stimulate host T cell function before total-body irradiation and transplantation. Given that mixed chimerism induces GVHD tolerance (32), host-residual iNKT cells may provide the attenuation of GVHD and the induction of mixed chimerism and graft rejection through a common mechanism that regulates graft-vs-donor immunity.

Induction of a Th2-dominant cytokine profile before the onset of obvious GVHD after transplantation (Fig. 2*B*) may, at least in part, be associated with such a mechanism, since many studies (33–35), with some conflicting reports (36, 37), have shown that Th2 cytokines protect against GVHD. In addition, some investigators have reported that IL-2, TNF-α, and IFN-γ play important roles in the development of GVHD in vivo (35, 38–41). Induction of cytokine production from residual iNKT cells by administration of α-GalCer or iNKT a few hours after transplantation was obvious. Th1 as well as Th2 cytokine secretion at the very early stage of transplantation may be favorable for balancing the recipients' and donors' T cell function and, as a result, may suppress GVHD. Besides, repeated α-GalCer administration may induce a Th2-dominant cytokine profile. These considerations, as well as previous reports that the GVHD-protective effect of NKT cells depends on IL-4 production from NKT cells (10–12, 14), support our speculation. Regarding other cytokines, several reports have noted that IL-12 (34, 42), IL-13 (43, 44), IL-15 (34, 38), and IL-18 (45) are

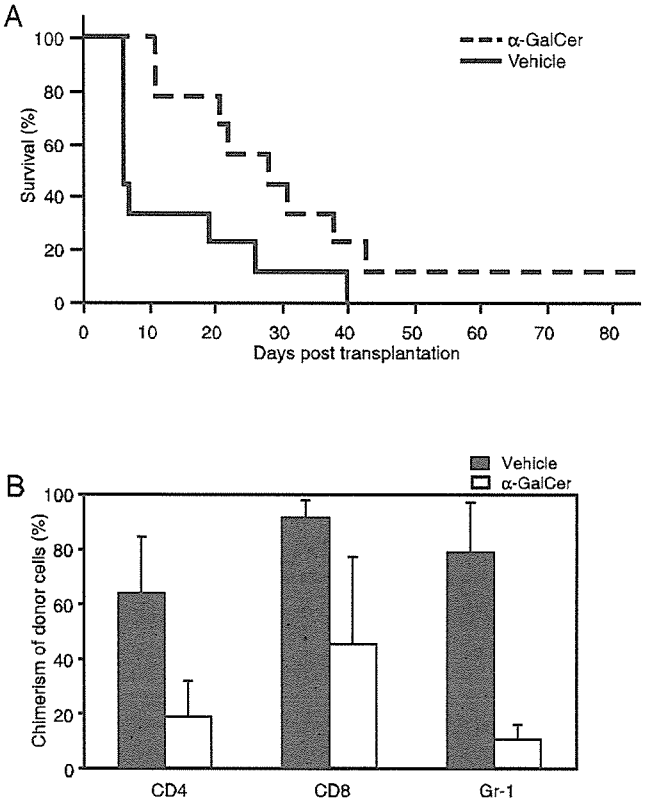

FIGURE 6. The prolongation of survival and graft rejection caused by α-GalCer treatment were unaffected by the depletion of NK cells. *A*, Survival of α-GalCer (n = 9)- and vehicle (n = 9)-treated wild-type BALB/c recipient mice. The mice were administered with anti-asialo GM1 Ab on day −1 of transplantation and transplanted with cells from wild-type C57BL/6 donor mice. α-GalCer was administered every 4 days from the day of transplantation. α-GalCer-treated mice survived longer than vehicle-treated mice (p = 0.005). Meantime, there was no difference between the anti-asialo GM1 Ab- and vehicle-administered groups (data not shown). *B*, Chimerism on day 7 of $CD4^+$ and $CD8^+$ splenocytes and Gr-1^+ bone marrow cells in α-GalCer and asialo GM1 Ab (n = 6)- and vehicle and asialo GM1 Ab (n = 4)-treated recipients. Asialo GM1 Ab was administered to the wild-type recipients on days −5 and −1, and α-GalCer was administered on days −4 and 0 of transplantation. Grafts were from $J\alpha18^{-/-}$ C57BL/6 mice. Significant differences were noted in each cell type ($CD4^+$, p = 0.002; $CD8^+$ and Gr-1^+, $p < 0.0001$).

also associated with GVHD. However, we could not obtain sufficient samples from sick mice to measure such various cytokines simultaneously. Although we were unable to evaluate all of these cytokines in this study, we hope we will be able to analyze a complete set of cytokines in future studies.

To further complicate this scenario, our findings also revealed that the absence of iNKT cells in the graft enhances the suppression of engraftment of donor cells. A simple interpretation of this result is that iNKT cells in the graft help donor cells engraft, which is apparently opposite to the effect of host-residual iNKT cells. While attenuating GVHD by inducing host-residual iNKT cells, graft-contaminated iNKT cells may suppress host-vs-graft immunity. We observed a delay of engraftment when we adoptively transferred iNKT cells expanded from the BALB/c strain while transplanting grafts from $J\alpha18^{-/-}$ C57BL/6 mice (data not shown). Furthermore, we observed high levels of serum cytokines after transplantation and in vitro-expanded iNKT cells only when recipients had iNKT cells. Therefore, these functional differences may simply depend on the place, tissue-residual iNKT cells or blood-borne iNKT cells that are pre-expanded in vitro. Under physiological conditions, the cytokine status could be created by iNKT cells in the liver to prevent autoreactivity, and this environment may be able to prevent GVHD and influence incoming iNKT cells to prevent the attack of the donor graft by the recipient lymphocytes. Alternatively, the suppression of graft-vs-host immunity by host-residual iNKT cells and the suppression of host-vs-graft immunity by graft-contaminated iNKT cells could also be explained by the recognition of non-self through members of Ly49 (46–48). At least NK cells, which were generally recognized as major effectors in graft rejection, are not the downstream effectors of iNKT cell-dependent graft rejection.

In the clinical setting, there is increasing interest in the kinetics of the establishment of donor chimerism because of the development of reduced intensity conditioning regimens for allogeneic stem cell transplantation. Our results suggest that recipient-residual iNKT cells play a role against the establishment of donor chimerism as well as in the prevention of GVHD. Warn us that α-GalCer must be used carefully to prevent or treat GVHD are the facts that the combination of overstimulation of recipient iNKT cells before transplantation and that the lack of iNKT cells in grafts can cause graft rejection.

In conclusion, host-residual iNKT cells have a regulatory function in GVHD. α-GalCer therapy has already been performed in clinical trials in cancer patients and was well tolerated (49). It may be attractive to use α-GalCer or iNKT cells therapeutically for the prevention or treatment of GVHD. However, care must be taken in its clinical application because of the possibility that the activation of host-residual iNKT cells could also increase graft rejection.

Acknowledgments

We thank M. Kronenberg (La Jolla Institute for Allergy and Immunology, La Jolla, CA) for agreeing to provide us with α-GalCer-loaded murine CD1d tetramer. We thank M. Harada (Chiba University, Chiba, Japan) for preparing $J\alpha18^{-/-}$ mice, T. Nakayama (Chiba University) for providing the Sf9 cell line and baculovirus-expressing mouse CD1d/β_2-microgloblin, and T. Ito (Chiba University) for considerable advice on the production of α-GalCer-loaded CD1d tetramers. We also thank E. Nagata and Y. Sato for providing excellent technical assistance.

Disclosures

The authors have no financial conflict of interest.

References

1. Godfrey, D., K. Hammond, L. Poulton, and A. Baxter. 2000. NKT cells: Facts, functions and fallacies. *Immunol. Today* 21: 573–583.
2. Wilson, M. T., A. K. Singh, and L. Kaer. 2002. Immunotherapy with ligands of natural killer T cells. *Trends Mol. Med.* 8: 225–231.
3. Fowlkes, B., A. Kruisbeek, H. Ton-That, M. Weston, J. Coligan, R. Schwartz, and D. Pardoll. 1987. A novel population of T cell receptor αβ-bearing thymocytes which predominantly express a single vβ8 gene family. *Nature* 329: 251–254.
4. Budd, R., G. Miescher, R. Howe, R. Lees, C. Bron, and H. MacDonald. 1987. Developmentally regulated expression of T cell receptor β chain variable domain is immature thymocytes. *J. Exp. Med.* 166: 577–582.
5. Dellabona, P., E. Padovan, G. Casorati, M. Brockhaus, and A. Lanzavecchia. 1994. An invariant Vα24-JαQ/Vβ11 T cell receptor is expressed in all individuals by clonally expanded $CD4^-CD8^-$ cells. *J. Exp. Med.* 180: 1171–1176.
6. Porcelli, S., D. Gerdes, A. Fertig, and S. Balk. 1996. Human T cells expressing an invariant Vα24-JαQ TCRα are CD4 $^-$and heterogenous with respect to TCRβ expression. *Hum. Immunol.* 48: 63–67.
7. Lantz, O., and A. Bendelac. 1994. An invariant T cell receptor α chain is used by a unique subset of major histocompatibility complex class I-specific $CD4^+$ and $CD4^-8^-$ T cells in mice and humans. *J. Exp. Med.* 180: 1097–1106.
8. Taniguchi, M., M. Harada, S. Kojo, T. Nakayama, and H. Wakao. 2003. The regulatory role of Vα14 NKT cells in innate and acquired immune response. *Annu. Rev. Immunol.* 21: 483–513.
9. Joyce, S. 2001. CD1d and natural T cells: How their properties jump-start the immune system. *Cell Mol. Life Sci.* 58: 442–469.
10. Zeng, D., D. Lewis, S. Dejbakhsh-Jones, F. Lan, M. Garcia-Ojeda, R. Sibley, and S. Strober. 1999. Bone marrow $NK1.1^-$ and $NK1.1^+$ T cells reciprocally regulate acute versus host disease. *J. Exp. Med.* 189: 1073–1081.

11. Lan, F., D. Zeng, M. Higuchi, P. Huie, J. P. Higgins, and S. Strober. 2001. Predominance of NK1.1$^+$TCR$\alpha\beta^+$ or DX5$^+$TCR$\alpha\beta^+$ T cells in mice conditioned with fractionated lymphoid irradiation protects against graft-versus-host disease: "natural suppressor" cells. *J. Immunol.* 167: 2087–2096.
12. Lan, F., D. Zeng, M. Higuchi, J. P. Higgins, and S. Strober. 2003. Host conditioning with total lymphoid irradiation and antithymocyte globulin prevents graft-versus-host disease: the role of CD1-reactive natural killer T cells. *Biol. Blood Marrow Transplant* 9: 355–363.
13. Morecki, S., S. Panigrahi, G. Pizov, E. Yacovlev, Y. Gelfand, O. Eizik, and S. Slavin. 2004. Effect of KRN7000 on induced graft-vs-host disease. *Exp. Hematol.* 32: 630–637.
14. Hashimoto, D., S. Asakura, S. Miyake, T. Yamamura, L. Van Kaer, C. Liu, M. Tanimoto, and T. Teshima. 2005. Stimulation of host NKT cells by synthetic glycolipid regulates acute graft-versus-host disease by inducing Th2 polarization of donor t cells. *J. Immunol.* 174: 551–556.
15. Haraguchi, K., T. Takahashi, K. Hiruma, Y. Kanda, Y. Tanaka, S. Ogawa, S. Chiba, O. Miura, H. Sakamaki, and H. Hirai. 2004. Recovery of Vα24$^+$ NKT cells after hematopoietic stem cell transplantation. *Bone Marrow Transplant* 34: 595–602.
16. Cui, J., T. Shin, T. Kawano, H. Sato, E. Kondo, I. Toura, Y. Kaneko, K. H., M. Kanno, and M. Taniguchi. 1997. Requirement for Vα14 NKT cells in IL-12-mediated rejection of tumors. *Science* 278: 1623–1626.
17. Matsuda, J. L., O. V. Naidenko, L. Gapin, T. Nakayama, M. Taniguchi, C.-R. Wang, Y. Koezuka, and M. Kronenberg. 2000. Tracking the response of natural killer T cells to a glycolipid antigen using CD1d tetramers. *J. Exp. Med.* 192: 741–754.
18. Smyth, M. J., N. Y. Crowe, D. G. Pellicci, K. Kyparissoudis, J. M. Kelly, K. Takeda, H. Yagita, and D. I. Godfrey. 2002. Sequential production of interferon-γ by NK1.1$^+$ T cells and natural killer cells is essential for the antimetastatic effect of α-galactosylceramide. *Blood* 99: 1259–1266.
19. Sharif, S., G. A. Arreaza, P. Zucker, Q.-S. Mi, J. Sondhi, O. V. Naidenko, M. Kronenberg, Y. Koezuka, T. L. Delovitch, J.-M. Gombert, et al. 2001. Activation of natural killer T cells by α-galactosylceramide treatment prevents the onset and recurrence of autoimmune type 1 diabetes. *Nat. Med.* 7: 1057.
20. Nakagawa, R., I. Nagafune, Y. Tazunoki, H. Ehara, H. Tomura, R. Iijima, K. Motoki, M. Kamishohara, and S. Seki. 2001. Mechanisms of the antimetastatic effect in liver and of the hepatocyte injury induced by α-galactosylceramide in mice. *J. Immunol.* 166: 6578–6584.
21. Chiodoni, C., A. Stoppacciaro, S. Sangaletti, G. Gri, B. Cappetti, Y. Koezuka, and Mario P. Colombo. 2001. Different requirements for α-galactosylceramide and rIL-12 antitumor activity in the treatment of C-26 colon carcinoma hepatic metastases. *Eur. J. Immunol.* 31: 3101–3110.
22. Cooke, K., L. Kobzik, T. Martin, J. Brewer, J. J. Delmonte, J. Crawford, and J. Ferrara. 1996. An experimental model of idiopathic pneumonia syndrome after bone marrow transplantation: I. The roles of minor H antigens and endotoxin. *Blood* 88: 3230–3239.
23. Singh, N., S. Hong, D. C. Scherer, I. Serizawa, N. Burdin, M. Kronenberg, Y. Koezuka, and L. Van Kaer. 1999. Cutting edge: Activation of NK T cells by CD1d and α-galactosylceramide directs conventional T cells to the acquisition of a Th2 phenotype. *J. Immunol.* 163: 2373–2377.
24. Chamoto, K., T. Takeshima, A. Kosaka, T. Tsuji, J. Matsuzaki, Y. Togashi, H. Ikeda, and T. Nishimura. 2004. NKT cells act as regulatory cells rather than killer cells during activation of NK cell-mediated cytotoxicity by α-galactosylceramide in vivo. *Immunol. Lett.* 95: 5–11.
25. Kaer, L. V. 2005. α-galactosylceramide therapy for autoimmune diseases: Prospects and obstacles. *Nat. Rev. Immunol.* 5: 31–42.
26. Burdin, N., L. Brossay, and M. Kronenberg. 1999. Immunization with α-galactosylceramide polarizes CD1-reactive NK T cells towards Th2 cytokine synthesis. *Eur. J. Immunol.* 29: 2014–2025.
27. Barao, I., and W. Murphy. 2003. The immunobiology of natural killer cells and bone marrow allograft rejection. *Biol. Blood Marrow Transplant* 9: 727–741.
28. Seino, K., K. Fukao, K. Muramoto, K. Yanagisawa, Y. Takada, S. Kakuta, Y. Iwakura, L. Kaer, K. Takeda, T. Nakayama, et al. 2001. Requirement for natural killer T (NKT) cells in the induction of allograft tolerance. *Proc. Natl. Acad. Sci. USA* 98: 2577–2581.
29. Chargui, J., T. Hase, S. Wada, T. Naganuma, and R. Yoshimura. 2001. NKT cells as nonspecific immune-regulator inducing tolerance in mouse model transplantation. *Transplant. Proc.* 33: 3833–3834.
30. Higuchi, M., D. Zeng, J. Shizuru, J. Gworek, S. Dejbakhsh-Jones, M. Taniguchi, and S. Strober. 2002. Immune tolerance to combined organ and bone marrow transplants after fractionated lymphoid irradiation involves regulatory NK T cells and clonal deletion. *J. Immunol.* 169: 5564–5570.
31. Ikehara, Y., Y. Yasunami, S. Kodama, T. Maki, M. Nkano, T. Nakayama, M. Taniguchi, and S. Ikeda. 2000. CD4$^+$ 1 Vα24 natural killer T cells are essential for acceptance of rat islet xenografts in mice. *J. Clin. Invest.* 105: 1761–1767.
32. Kolb, H.-J., C. Schmid, X. Chen, A. Woiciechowski, M. Roskrow, M. Weber, W. Guenther, G. Ledderose, and M. Schleuning. 2003. Adoptive immunotherapy in chimeras with donor lymphocytes. *Acta Haematol.* 110: 110–120.
33. Fowler, D. H., and R. E. Gress. 2000. Th2 and Tc2 cells in the regulation of GVHD, GVL, and graft rejection: considerations for the allogeneic transplantation therapy of leukemia and lymphoma. *Leuk. Lymphoma* 38: 221–234.
34. Teshima, T., and J. Ferrara. 2002. Understanding the alloresponse: new approaches to graft-versus-host disease prevention. *Semin. Hematol.* 39: 15–22.
35. Goker, H., I. C. Haznedaroglu, and N. J. Chao. 2001. Acute graft-vs-host disease: pathobiology and management. *Exp. Hematol.* 29: 259–277.
36. Murphy, W. J., L. A. Welniak, D. D. Taub, R. H. Wiltrout, P. A. Taylor, D. A. Vallera, M. Kopf, H. Young, D. L. Longo, and B. R. Blazar. 1998. Differential effects of the absence of interferon-γ and IL-4 in acute graft-versus-host disease after allogeneic bone marrow transplantation in mice. *J. Clin. Invest.* 102: 1742–1748.
37. Nikolic, B., S. Lee, R. T. Bronson, M. J. Grusby, and M. Sykes. 2000. Th1 and Th2 mediate acute graft-versus-host disease, each with distinct end-organ targets. *J. Clin. Invest.* 105: 1289–1298.
38. Reddy, P., and J. L. M. Ferrara. 2003. Immunobiology of acute graft-versus-host disease. *Blood Rev.* 17: 187–194.
39. Shalaby, M. R., B. Fendly, K. C. Sheehan, R. D. Schreiber, and A. J. Ammann. 1989. Prevention of the graft-versus-host reaction in newborn mice by antibodies to tumor necrosis factor-α. *Transplantation* 47: 1057–1061.
40. Via, C. S., and F. D. Finkelman. 1993. Critical role of interleukin-2 in the development of acute graft-versus-host disease. *Int. Immunol.* 5: 565–572.
41. Mowat, A. 1989. Antibodies to IFN-γ prevent immunologically mediated intestinal damage in murine graft-versus-host reaction. *Immunology* 68: 18–23.
42. Deeg, H. J. 2001. Cytokines in graft-versus-host disease and the graft-versus-leukemia reaction. *Int. J. Hematol.* 74: 26–32.
43. Jordan, W. J., P. A. Brookes, R. M. Szydlo, J. M. Goldman, R. I. Lechler, and M. A. Ritter. 2004. IL-13 production by donor T cells is prognostic of acute graft-versus-host disease following unrelated donor stem cell transplantation. *Blood* 103: 717–724.
44. Imamura, M., Y. Tsutsumi, Y. Miura, T. Toubai, and J. Tanaka. 2003. Immune reconstitution and tolerance after allogeneic hematopoietic stem cell transplantation. *Hematology* 8: 19–21.
45. Holler, E. 2002. Cytokines, viruses, and graft-versus-host disease. *Curr. Opin. Hematol.* 9: 479–484.
46. Maeda, M., S. Lohwasser, T. Yamamura, and F. Takei. 2001. Regulation of NKT cells by Ly49: Analysis of primary NKT cells and generation of NKT cell line. *J. Immunol.* 167: 4180–4186.
47. Ikarashi, Y., R. Mikami, A. Bendelac, M. Terme, N. Chaput, M. Terada, T. Tursz, E. Angevin, F. A. Lemonnier, H. Wakasugi, and L. Zitvogel. 2001. Dendritic cell maturation overrules H-2D-mediated natural killer T (NKT) cell inhibition: Critical role for B7 in CD1d-dependent NKT cell interferon γ production. *J. Exp. Med.* 194: 1179–1186.
48. Hayakawa, Y., S. Berzins, N. Crowe, D. Godfrey, and M. Smyth. 2004. Antigen-induced tolerance by intrathymic modulation of self-recognizing inhibitory receptors. *Nat. Immunol.* 5: 590–596.
49. Giaccone, G., C. J. A. Punt, Y. Ando, R. Ruijter, N. Nishi, M. Peters, B. M. E. von Blomberg, R. J. Scheper, H. J. J. van der Vliet, A. J. M. van den Eertwegh, et al. 2002. A Phase I study of the natural killer T-cell ligand α-galactosylceramide (KRN7000) in patients with solid tumors. *Clin. Cancer Res.* 8: 3702–3709.

Table 1 Patient clinical features

Clinical features	*Diagnosis (November 1998)*	*Disease progression (November 2001)*	*Disease recurrence (February 2004)*	*B hepatitis onset (September 2004)*
Rai clinical stage	I	II	II	0
CD38	Negative	Negative	Negative	Negative
Zap 70	Positive	Positive	Positive	Negative
CD4/CD8	0.95	0.90	0.85	0.80
Beta 2 microglobulin (mcg/l)	1503	1825	1844	1325
Serum Ig level (g/l)	0.980	0.790	0.660	0.620
HBsAg	Negative	Negative	Negative	Negative
HBsAb	Negative	Negative	Negative	Negative
HBcAb	Positive	Positive	Positive	Positive
HBeAg	Negative	Negative	Negative	Positive
HBeAb	Positive	Positive	Positive	Positive
HBV DNA	NA	NA	NA	200.000/μl

Ig: immunoglobulin.

followed up until about 2 years later (February 2004) when, for a disease recurrence, rituximab was given again.

At this time, all the above hepatitis markers remained unmodified. After four weekly standard doses of rituximab a GPR was recorded, and then six monthly courses (150 mg/m^2) of the same agent were administered as maintenance therapy. In September 2004, being the patient in CR, he was admitted with acute hepatitis. HBV DNA strains (200 000 copies/ml) were detected, whereas the HbsAg-negative status persisted.

Under antiviral treatment with lamivudine, the viraemia decreased to 3300 copies/ml within 2 weeks. Nevertheless, hepatic function did not recover, and the patient died 32 days after his admission.

Although reactivation of HBV in HBsAg-positive patients is a well-documented complication of cytotoxic treatments,[4,5] to the best of our knowledge, this is the first case of HBV reactivation in a B-CLL patient after rituximab. Moreover, we recorded the presence of HBcAb and HBeAb associated with the negativity of HbsAg and HBsAb, indicating that these findings are a long-lasting occult infection of a HBV variant strain. Given the high efficacy of prophylaxis with lamivudine, testing HBV DNA before immunosuppressive and cytotoxic treatments, including the anti-CD20 antibodies, should be recommended in order to identify HBV carriers among patients presenting HBcAb alone without any other serological HBV markers, since HBsAg routine tests may be unreliable in S-gene mutated variants.

P Niscola[1]
MI Del Principe[1]
L Maurillo[1]
A Venditti[1]
F Buccisano[1]
D Piccioni[1]
S Amadori[1]
G Del Poeta[1]

[1]*Department of Hematology, Tor Vergata University, Rome, Italy*

References

1 Dervite I, Hober D, Morel P. Acute hepatitis B in a patient with antibodies to hepatitis B surface antigen who was receiving rituximab. *N Engl J Med* 2001; **344**: 68–69.
2 Westhoff TH, Jochimsen F, Schmittel A, Stoffler-Meilicke M, Schafer JH, Zidek W *et al.* Fatal hepatitis B virus reactivation by an escape mutant following rituximab therapy. *Blood* 2003; **102**: 1930.
3 Ng HJ, Lim LC. Fulminant hepatitis B virus reactivation with concomitant listeriosis after fludarabine and rituximab therapy: case report. *Ann Hematol* 2001; **80**: 549–552.
4 Picardi M, Pane F, Quintarelli C, De Renzo A, Del Giudice A, De Divitiis B *et al.* Hepatitis B virus reactivation after fludarabine-based regimens for indolent non-Hodgkin's lymphomas: high prevalence of acquired viral genomic mutations. *Haematologica* 2003; **88**: 1296–1303.
5 Tsutsumi Y, Tanaka J, Kawamura T, Miura T, Kanamori H, Obara S *et al.* Possible efficacy of lamivudine treatment to prevent hepatitis B virus reactivation due to rituximab therapy in a patient with non-Hodgkin's lymphoma. *Ann Hematol* 2004; **83**: 58–60.

Mutations of the Notch1 gene in T-cell acute lymphoblastic leukemia: analysis in adults and children

Leukemia (2005) **19**, 1841–1843. doi:10.1038/sj.leu.2403896; published online 4 August 2005

TO THE EDITOR

Notch signaling plays a key role in the cell fate decision at various differentiation branch points.[1] In mammals, it has been well recognized that the deregulated activation of Notch signaling leads to tumor development.[2] This concept is highlighted by a recent report demonstrating that as much as 60% of childhood T-cell acute lymphoblastic leukemia (T-ALL) has mutations in the *Notch1* gene.[3] The resulting amino-acid changes have been found in the heterodimerization (HD) domains at the C- and N-termini of the extracellular and transmembrane subunits (HD^{EC} and HD^{TM} domains), respectively, and the transcriptional activation (TA) and PEST domains at the cytoplasmic region of the transmembrane subunit. The former mutations are thought to reduce the affinity between the two subunits, which subsequently leads to ligand-independent γ-cleavage of the Notch1 transmembrane subunit and production of an activated Notch1 intracellular domain. In the latter, insertion or deletion mutations introduce a premature stop codon that results in truncation of the PEST domain, which

Correspondence: Dr S Chiba, Department of Cell Therapy and Transplantation Medicine, University of Tokyo Hospital, 7-3-1 Hongo, Bunkyo-ku, Tokyo 113-8655, Japan; Fax: +81 3 5689 7286;
E-mail: schiba-tky@umin.ac.jp
Received 13 June 2005; accepted 28 June 2005; published online 4 August 2005

eventually causes prolonged half-life of the cleaved Notch1 intracellular domain. Both mutations appear to result in activation of Notch signaling and initiate or develop leukemia.[3] Extremely high frequency of activating mutations of the *Notch1* gene gave us an idea that T-ALL is commonly dependent on abnormal Notch1 activation. Based on these findings, it has been postulated that γ-secretase inhibitors, which are considered as a treatment modality against Alzheimer's disease,[4] could be useful as anti-T-ALL drugs.

While adult T-ALL has pathological characteristics common to childhood T-ALL, some differences have been recognized from both clinical observations[5] and molecular studies.[6] Therefore, it would be worthwhile to examine *Notch1* mutations in adult T-ALL to gain insight into the entity and subclassification of T-ALL, based on the knowledge of exceptionally high frequency of *Notch1* mutations in childhood T-ALL.

In the current study, we found that *Notch1* mutations were frequent in both adult and childhood T-ALLs. In the 14 adult T-ALL samples, we found an in-frame 3-nucleotide deletion mutation in one and an in-frame 3-nucleotide insertion mutation in another in the HD^{EC} domain. The former was described in the previous report as one of the 'hot spots' that leads to the deletion of 1579V. In the latter (Figure 1, upper panel), Gly was inserted between amino-acids 1597L and 1598S. Although the same mutation was not described in the previous report, these two residues are conserved among the vertebrate *Notch1* gene products, and thus 1598 Ins G may also cause ligand-independent activation of Notch1. In the $HD^{™}$ domain, we found a missense mutation 1681I/N in one case, which was described in children (Figure 1, middle panel). In the TA domain, there was a mutation with a 3-nucleotide deletion and a 4-nucleotide insertion at the same position, resulting in a frame shift and a premature stop codon (Figure 1, lower panel). In the PEST domain, there was a mutation with a 5-nucleotide insertion, also resulting in a premature termination of translation. Both of these insertion mutations lead to truncation of the PEST domain.

Overall, we found five potentially activating mutations in five adult patients, among 14, with ages of 17, 19, 24, 31 and 37 years (summarized in Table 1). No sample showed mutations at both the HD and PEST domains, most likely because of the small sample number.

In 10 out of the 14 adults analyzed, we previously studied the deletion of *CDKN2A* antioncogene. Although homozygous deletion of this gene, which is known to be frequent in childhood T-ALL, was found in only one of these 10 cases,[7] we also found an activating *Notch1* mutation in the HD domain in the same sample. From this observation, we can conclude that activating mutation of *Notch1* gene and inactivation of *CDKN2A* gene, which are the most frequent abnormalities in T-ALL, are not likely to be mutually exclusive.

We also analyzed the *Notch1* gene in 33 childhood T-ALL samples. We found 12, 3 and 2 mutations in the HD^{EC}, $HD^{™}$

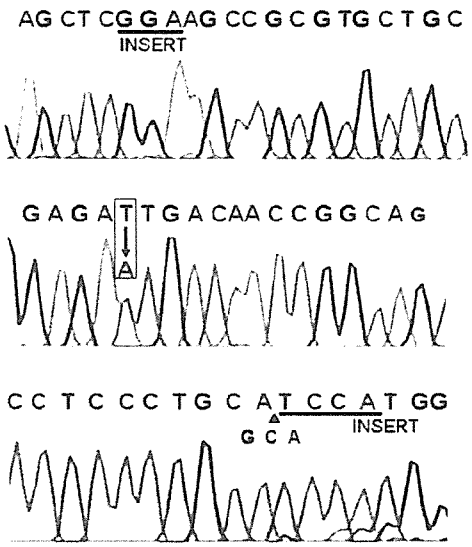

Figure 1 Sequence analysis of adult T-ALL patients. (upper panel) Insertion at 4792, GGA (HD^{EC} domain); (middle panel) missense mutation at 5042, T→A ($HD^{™}$ domain); (lower panel) deletion at 7032, GCA, and insertion at the same position, TCCA.

Table 1 Notch1 heterodimerization domain and PEST domain mutational status and deletion of *CDKN2A* gene in primary T-ALL cells from adult patients

ID	*Age (years)*	*CDKN2A*	*Notch1*	*Seq HD domain*	*Mut HD domain*	*Seq PEST domain*	*Mut PEST domain*
T-ALL 1	20	+/+	WT	SNP 5097 C/T	—	—	—
T-ALL 2	31	+/+	**Mut**	**{5042 T/A** SNP 5097 C/T}	**1681 I/N**	—	—
T-ALL 3	18	+/+	WT	SNP 5097 C/T	—	—	—
T-ALL 4	72	+/+	WT	SNP 5097 C/T	—	—	—
T-ALL 5	19	+/+	**Mut**	SNP 5097 C/T	—	**Ins. 7374 ATTCT**	**2458 LFCPRRAPPCPRRCHPRWSHPStop**
T-ALL 6	19	+/+	WT	SNP 5097 C/T	—	—	—
T-ALL 7	24	+/+	**Mut**	SNP 5097 C/T	—	**{Del. 7032 GCA Ins. 7035 TCCA}**	**2344 HPWHGRPAAQStop**
T-ALL 8	17	**−/−**	**Mut**	**{Ins. 4792 GGA** SNP 5097 C/T}	**1598 Ins. G**	—	—
T-ALL 9	42	+/+	WT	SNP 5097 C/T	—	—	—
T-ALL 10	68	+/+	WT	SNP 5097 C/T	—	—	—
T-ALL 11	65	ND	WT	SNP 5097 C/T	—	—	—
T-ALL 12	37	ND	**Mut**	**{Del. 4735 GTG** SNP 5097 C/T}	**1579 Del. V**	—	—
T-ALL 13	17	ND	WT	—	—	—	—
T-ALL 14	55	ND	WT	SNP 5097 C/T	—	—	—

Seq = sequence; HD = heterodimerization domain; Mut = mutation; WT = wild-type; Ins = insertion; Del = deletion; +/+, no deletion; −/−, homozygous deletion; ND = not determined.
Bold indicate samples which have a mutation.

and PEST domains, respectively (data not shown). Overall, we found 17 mutations in 16 of 33 childhood T-ALL cases (48.5%), recapitulating the previous observation.[3]

It is intriguing to consider γ-secretase inhibitors as antileukemia agents, with Notch signaling being a new therapeutic target, since their efficacy is predicted and there are ongoing clinical trials of γ-secretase inhibitors as anti-Alzheimer drugs. However, at least two issues must be considered further.

First, according to the previous report, many *Notch1*-mutated T-ALL cell lines are not likely to respond to γ-secretase inhibitors, although some are definitely sensitive to these agents. Indeed, we found that γ-secretase inhibitors that induce apoptosis in some T-ALL cell lines did not affect many *Notch1*-mutated T-ALL cell lines despite the fact that these γ-secretase inhibitors unambiguously blocked the activation of Notch1 (data not shown). These findings indicate that Notch1 activation is not always required for the growth of T-ALL cell lines even if they have mutations. This may be due to additional mutations during establishment of the cell line or presense of Notch-independent cell growth machinery in T-ALL cells from patients. To see whether Notch signaling is a good therapeutic target, it is important to examine fresh T-ALL cells for frequency of responsiveness to γ-secretase inhibitors.

Second, with the development of γ-secretase inhibitors for the treatment of Alzheimer's disease, major effort has been made to find compounds that have less effect on Notch signaling. Indeed, it has been clearly shown that the administration of large amounts of Ly411575, a compound with a strong γ-secretase inhibiting activity, to mice induces severe abnormalities in the immune system and digestive tract.[8] Therefore, it is unlikely that we can divert a γ-secretase inhibitor that has been developed for treatment of Alzheimer's disease to an anti-T-ALL drug. We need a careful strategy to find γ-secretase inhibitors or other Notch inhibitors that could be used for T-ALL and potentially other malignancies, with acceptable side effects due to the inhibition of Notch signaling, which is required for cell life physiologically.

Acknowledgements

This work was supported in part by Grant-in-Aid for Scientific Research on Priority Areas, KAKENHI-17013022 (to SO) and KAKENHI-17390274 (to SC) from the Ministry of Education, Culture, Sports, Science and Technology of Japan, and by Japan Health Sciences Foundation (to SC).

S-Y Lee[1]
K Kumano[1,2]
S Masuda[1,2]
A Hangaishi[2]
J Takita[4]
K Nakazaki[2]
M Kurokawa[2]
Y Hayashi[5]
S Ogawa[2,3]
S Chiba[1,2]

[1]*Department of Cell Therapy and Transplantation Medicine, University of Tokyo, Tokyo, Japan;*
[2]*Department of Hematology and Oncology, University of Tokyo, Tokyo, Japan;*
[3]*Department of Regeneration Medicine for Hematopoiesis, University of Tokyo, Tokyo, Japan*
[4]*Department of Pediatrics, University of Tokyo, Tokyo, Japan; and*
[5]*Department of Hematology and Oncology, Gunma Children's Medical Center, Gunma, Japan*

References

1 Artavanis-Tsakonas S, Rand MD, Lake RJ. Notch signaling: cell fate control and signal integration in development. *Science* 1999; **284**: 770–776.
2 Radtke F, Raj K. The role of Notch in tumorigenesis: oncogene or tumour suppressor? *Nat Rev Cancer* 2003; **3**: 756–767.
3 Weng AP, Ferrando AA, Lee W, Morris IV JP, Silverman LB, Sanchez-Irizarry C *et al.* Activating mutations of NOTCH1 in human T cell acute lymphoblastic leukemia. *Science* 2004; **306**: 269–271.
4 Wolfe MS. Therapeutic strategies for Alzheimer's disease. *Nat Rev Drug Discov* 2002; **1**: 859–866.
5 Hoelzer D, Gokbuget N. New approaches to acute lymphoblastic leukemia in adults: where do we go? *Semin Oncol* 2000; **27**: 540–559.
6 Aplan PD. Adults are not simply big children. *Blood* 2004; **103**: 2437–2438.
7 Ogawa S, Hangaishi A, Miyawaki S, Hirosawa S, Miura Y, Takeyama K *et al.* Loss of the cyclin-dependent kinase 4-inhibitor (p16; MTS1) gene is frequent in and highly specific to lymphoid tumors in primary human hematopoietic malignancies. *Blood* 1995; **86**: 1548–1556.
8 Wong GT, Manfra D, Poulet FM, Zhang Q, Josien H, Bara T *et al.* Chronic treatment with the gamma-secretase inhibitor LY-411,575 inhibits beta-amyloid peptide production and alters lymphopoiesis and intestinal cell differentiation. *J Biol Chem* 2004; **279**: 12876–12882.

JAK2 Val617Phe activating tyrosine kinase mutation in juvenile myelomonocytic leukemia

Leukemia (2005) **19**, 1843–1844. doi:10.1038/sj.leu.2403903; published online 4 August 2005

TO THE EDITOR

Juvenile myelomonocytic leukemia (JMML) is a rare myeloproliferative/myelodysplastic disorder of early childhood.[1] Genetic abnormalities of the three genes *RAS* (15–20%), neurofibromatosis type I (*NF1*) (25%), and protein-tyrosine phosphatase, nonreceptor type 11 (*PTPN11*) (34%), all of which are positioned in the GM-CSF/Ras signal transduction pathway, have been implicated in the pathogenesis of JMML.[2–4] One of these genetic abnormalities is observed in 75% of JMML patients, leaving 25% of the reported cases in which a specific mutation has yet to be detected. Recent reports described an acquired mutation of the tyrosine kinase *JAK2* gene that has been found in human myeloproliferative disorders, and the single-point mutation (Val617Phe) in exon 12 was identified.[5–7] Several data demonstrate that JAK2 is physically associated with the GM-CSFRβ chain, becoming activated upon challenge of myeloid cells with GM-CSF.[8] To clarify the involvement of JAK2 in the pathogenesis of JMML, we searched for mutations in the *JAK2* gene in five JMML patients.

The diagnosis of JMML for each patient was confirmed according to diagnostic criteria agreed upon by the International JMML Working Group.[1] Genomic DNA was extracted from patients' bone marrow cells, and the human *JAK2* exon 12 was

Correspondence: Dr E Ito, Department of Pediatrics, Hirosaki University School of Medicine, 53 Honcho, Hirosaki, Aomori, 036-8563, Japan; Fax: 81 172 39 5071; E-mail: eturou@cc.hirosaki-u.ac.jp
Received 13 June 2005; accepted 5 July 2005; published online 4 August 2005

Am J Physiol Endocrinol Metab 289: E419–E428, 2005.
First published April 12, 2005; doi:10.1152/ajpendo.00512.2004.

Proteomic analysis on insulin signaling in human hematopoietic cells: identification of CLIC1 and SRp20 as novel downstream effectors of insulin

Kumiko Saeki,[1]* Etsuko Yasugi,[1]* Emiko Okuma,[1] Samuel N. Breit,[4] Megumi Nakamura,[3] Tosifusa Toda,[3] Yasushi Kaburagi,[2] and Akira Yuo[1]

[1]*Departments of Hematology and* [2]*Metabolic Disorder, Research Institute, International Medical Center of Japan;* [3]*Proteomics Collaboration Research Group, Tokyo Metropolitan Institute of Gerontology, Tokyo, Japan; and* [4]*Centre for Immunology, St. Vincent's Hospital, and University of New South Wales, Sydney, Australia*

Submitted 27 October 2004; accepted in final form 11 April 2005

Saeki, Kumiko, Etsuko Yasugi, Emiko Okuma, Samuel N. Breit, Megumi Nakamura, Tosifusa Toda, Yasushi Kaburagi, and Akira Yuo. Proteomic analysis on insulin signaling in human hematopoietic cells: identification of CLIC1 and SRp20 as novel downstream effectors of insulin. *Am J Physiol Endocrinol Metab* 289: E419–E428, 2005. First published April 12, 2005; doi:10.1152/ajpendo.00512.2004.—Insulin/IGF-I-dependent signals play important roles for the regulation of proliferation, differentiation, metabolism, and autophagy in various cells, including hematopoietic cells. Although the early protein kinase activation cascade has been intensively studied, the whole picture of intracellular signaling events has not yet been clarified. To identify novel downstream effectors of insulin-dependent signals in relatively early phases, we performed high-resolution two-dimensional electrophoresis (2-DE)-based proteomic analysis using human hematopoietic cells 1 h after insulin stimulation. We identified SRp20, a splicing factor, and CLIC1, an intracellular chloride ion channel, as novel downstream effectors besides previously reported effectors of Rho-guanine nucleotide dissociation inhibitor 2 and glutathione *S*-transferase-pi. Reduction in SRp20 was confirmed by one-dimensional Western blotting. Moreover, MG-132, a proteasome inhibitor, prevented this reduction. By contrast, upregulation of CLIC1 was not observed in one-dimensional Western blotting, unlike the 2-DE results. As hydrophilic proteins were predominantly recovered in 2-DE, the discrepancy between the 1-DE and 2-DE results may indicate a certain qualitative change of the protein. Indeed, the nuclear localization pattern of CLIC1 was remarkably changed by insulin stimulation. Thus insulin induces the proteasome-dependent degradation of SRp20 as well as the subnuclear relocalization of CLIC1.

HL-60 cells; PDQuest; matrix-assisted laser desorption ionization coupled to time-of-flight mass spectrometry; Mascot

INSULIN AND INSULIN-LIKE GROWTH FACTOR I (IGF-I) are known as important regulators of a variety of biological effects, including growth, development, and metabolism. Moreover, insulin-dependent signals contribute to the regulation of azurophil granule-selective macroautophagy in human hematopoietic cells (16). The molecular mechanisms for the actions of insulin and IGF-I have been intensively studied by various approaches, including gene-targeting animal experiments (1, 8, 14, 22) and molecular cloning techniques (20, 21). Now, the scenario for early intracellular signal transduction including a protein kinase activation cascade is well documented. It has been revealed that common intracellular signaling pathways are working downstream of insulin and IGF-I, including insulin receptor substrates (IRSs) (12) and Shc (17). The IRSs phosphorylate phosphatidylinositol 3-kinase to activate Akt, which transmits signals for proliferation and survival as well as the hematopoietic macroautophagy regulation (16), and the mammalian target of rapamycin and S6 kinase, which transmit signals for growth and translation besides heaptic macroautophagy regulation (2). On the other hand, Shc transmits signals for differentiation in hematopoietic cells (25).

In contrast to the early signal transduction, the picture of the later signaling events remains rather obscure. A large number of still undetermined molecules may be working downstream of the insulin-dependent signals. To obtain the whole picture of the intracellular signaling events downstream of the insulin receptor, comprehensive studies such as transcriptome analysis and proteome analysis may be especially powerful. A transcriptome analysis can illuminate the intracellular signaling events if they require new transcriptions or altered message stabilities. However, changes in protein expression are not always associated with those of the message expression, and vice versa. Thus transcriptome analysis would occasionally bring about false positive and/or false negative results. In this sense, proteome analysis is thought to be a more practical tool. Moreover, proteome analysis has merit in demonstrating protein modification changes such as phosphorylation and acetylation besides the change in net expression amounts. Indeed, studies on proteome analysis have successfully identified the protein molecules associated with metabolic regulation in the liver (3, 7). However, proteome analysis on insulin signaling in hematopoietic cells has not been performed despite the significance of insulin-dependent signals in the hematopoietic system.

For the first time, we performed proteomic analysis using human hematopoietic cells with the high-resolution two-dimensional electrophoresis (2-DE) system. We show that SRp20, a splicing factor, and CLIC1, an intracellular chloride ion channel, are working as novel downstream effectors of insulin signaling. The biological relevance of these events is discussed.

MATERIALS AND METHODS

Cells, growth factors, and inhibitors. HL-60 cells were maintained in RPMI 1640 medium (Life Technologies, Grand Island, NY) supplemented with 10% heat-inactivated fetal calf serum (FCS; JRH Bioscience, Lenexa, KS). For insulin-stimulating experiments, cells

* These authors contributed equally to this work. The order of the authors' names was arbitrarily arranged.

Address for reprint requests and other correspondence: A. Yuo, Dept. of Hematology, Research Institute, International Medical Center of Japan, 1-21-1 Toyama, Shinjuku-ku, Tokyo 162-8655, Japan (e-mail: yuoakira@ri.imcj.go.jp).

The costs of publication of this article were defrayed in part by the payment of page charges. The article must therefore be hereby marked "*advertisement*" in accordance with 18 U.S.C. Section 1734 solely to indicate this fact.

had been previously cultured in serum-free RPMI 1640 medium supplemented with 5 μg/ml human holo-transferrin (Sigma Chemical, St. Louis, MO) for 3 days, and then 5 μg/ml insulin (Sigma) were added. Transferrin was suspended in RPMI 1640 medium, and insulin was solubilized by 1 N hydrochloride. In some experiments, MG-132 (Calbiochem, La Jolla, CA) was added 30 min before insulin stimulation.

Two-dimensional gel electrophoresis with quantitative analyses. Insulin-depleted cells were stimulated by insulin. After a 1-h incubation, stimulated and nonstimulated cells were collected. After a washing with wash buffer (10 mM Tris·HCl buffer, pH 8.0, 5 mM magnesium acetate), 4×10^7 cells were suspended with 7 volumes of lysis buffer containing 2 M thiourea, 7 M urea, 4% (wt/vol) CHAPS, and 1 mM Pefabloc SC PLUS (Roche Diagnostics, Mannheim, Germany). The cell suspensions were kept for 10 min on ice, sonicated intermittently, and centrifuged at 12,000 *g* for 10 min at 4°C, and the supernatant fractions were collected. The protein concentration was determined in the lysis solution with a dye reagent from Amersham Biosciences (Piscataway, NJ), using BSA as a standard. The lysate was alkylated with Ready Prep Reduction-Alkylation Kit (Bio-Rad Laboratories, Hercules, CA). The 120 μg of protein lysate per gel were subjected to two-dimensional gel electrophoresis (2-DE). One-dimensional isoelectric focusing was carried out using Immobiline dry strip (18 cm long, pH 3–10 nonlinear or pH 4–7 linear, Amersham Biosciences) in a horizontal electrophoresis system (Ettan IPGphor, Amersham Biosciences) according to the manufacturer's instructions. After the one-dimensional electrofocusing, IPG gels were equilibrated with buffer containing 50 mM Tris·HCl (pH 8.8), 6 M urea, 30% (vol/vol) glycerol, 2% (wt/vol) sodium dodecyl sulfate (SDS), 0.01% bromophenol blue, and 0.5% dithiothreitol, followed by alkylation with equilibration buffer containing 4.5% idoacetamide instead of 0.5% dithiothreitol at room temperature for 15 min. The gels were subjected to two-dimensional SDS-PAGE (10% gel). Proteins were visualized in the gels by staining with SYPRO Ruby Protein Gel Stain (Bio-Rad Laboratories) for overnight. The florescence intensity of each protein spot was digitally recorded by FluorImager 595 (Amersham Biosciences) using ImageQuaNT software and the differential protein expression quantitatively analyzed by PDQuest software (Bio-Rad Laboratories). The density of each spot was normalized by that of the smallest β-actin spot. Initially, all of the spots were roughly matched by an automatic program in PDQuest software, which was followed by a more detailed manual matching process to correct inappropriate matching pairs. Three to six independent experiments were performed, and the results were statistically analyzed by Student's *t*-test.

Mass spectrometric analysis. Mass spectrometric analysis was performed according to the method reported by Toda et al. (23), with slight modifications. Briefly, each protein spot in SYPRO Ruby-stained gels was picked by FluoroPhoreStar 3000 (Anatech, Tokyo, Japan). The pieces of gels were dehydrated in 50% acetonitrile and 50% ammonium bicarbonate, next in 100% acetonitrile, and dried. The proteins were digested with 5 μg/ml trypsin (sequencing grade modified trypsin; Promega, Madison, WI) at 30°C. After overnight protein digestion, peptide fragments in the digest were subjected to matrix-assisted laser desorption ionization (MALDI) coupled to a time-of-flight (TOF) (MALDI-TOF) mass spectrometer (AXIMA-CFR; Shimazdu, Kyoto, Japan) for peptide mass fingerprinting (PMF). Protein identification was performed with the Mascot server (Matrix Science, Boston, MA) and Protein Prospector (UCSF Mass Spectrometry Facility, San Francisco, CA). We selected the *Homo sapiens* database of SWISS-PROT and parameters: peptide tolerance ± 0.4 Da and one missed cleavage. Carbamidomethyl modification of cysteine and acetylation of the NH_2-terminal end or lysine and phosphorylation of serine, threonine, or tyrosine were considered. Protein identification was repeated at least once with spots from different gels. Phosphorylated peptides were confirmed by MALDI-TOF-MS in a postsource decay (PSD) mode of AXIMA-CFR and AXIMA-CFRplus (Shimadzu). NH_2-terminal acetylation was determined by MALDI-QIT-TOF-MS in an MS/MS mode (AXIMA-QIT, Shimadzu).

One-dimensional Western blotting. Cells (5×10^5) were lysed with 100 μl of 1× Laemmli's sample buffer and boiled. Ten microliters of this lysate were subjected to SDS-PAGE with 15% gels. The electric transfer onto a polyvinylidene difluoride (PVDF) membrane was carried out with a semidry blotting apparatus (Bio-Rad Laboratories) at 50 mA/cm^2 for 45 min at room temperature using buffer containing 2.25% Tris, 10.8% glycine, and 20% methanol. The first antibody reaction was performed using anti-SRp20 antibody (7B4; Santa Cruz Biotechnology, Santa Cruz, CA), anti-Rho-guanine nucleotide dissociation inhibitor (Rho-GDI) antibody (A-20; Santa Cruz Biotechnology), anti-β-tubulin antibody (H-235; Santa Cruz Biotechnology), a sheep anti-CLIC1 antiserum (25), anti-cyclin D3 antibody (C-16; Santa Cruz Biotechnology), anti-cyclin E antibody (M-20; Santa Cruz Biotechnology), and anti-cyclin A antibody (BF683; Upstate Biotechnology, Lake Placid, NY). The second antibody reaction and the final detection procedure were performed using ECL Western blotting detection reagents (Amersham Biosciences) or SuperSignal West Dura Extended Duration Substrate (Pierce Biotechnology, Rockford, IL) according to the manufacturers' guidance. Information of the chemical luminescence was analogically developed onto Hyperfilm (Amersham Biosciences). After scanning of the developed film, the band intensities were calculated by ImageQuant software (Amersham Biosciences). Stripping of the first antibody was performed by incubating the PVDF membrane with Restore Western Blot Stripping Buffer (Pierce Biotechnology) at room temperature for 30 min.

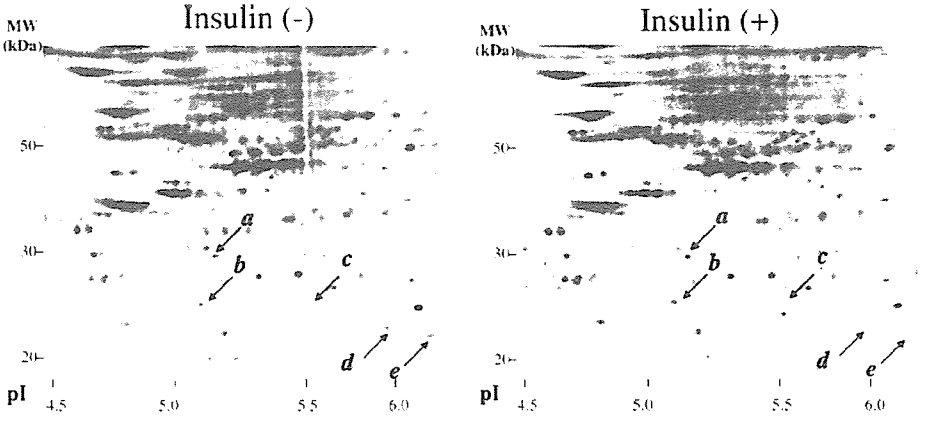

Fig. 1. Two-dimensional electrophoresis (2-DE) profile of human hematopoietic HL-60 cells with or without insulin treatment. HL-60 cells were cultured with transferrin-supplemented serum-free medium for 3 days. Then buffer solution (*left*) or 5 μg/ml insulin (*right*) was added, and cells were cultured for another 1 h at 37°C. Cell lysates were prepared as described in Experimental Procedures, and 2-DE was carried out. PDQuest software-based analysis demonstrated that the 5 spots (indicated by arrows) showed significant differences in their expressions with or without insulin treatment. *Spot a*, CLIC1, an intracellular chloride ion channel; *spot b*, Rho-guanine nucleotide dissociation inhibitor 2 (Rho-GDI-1); *spot c*, and glutathione *S*-transferase-pi (GST-pi); *spots d* and *e*, SRp-20, a splicing factor; *isoform of β-actin.

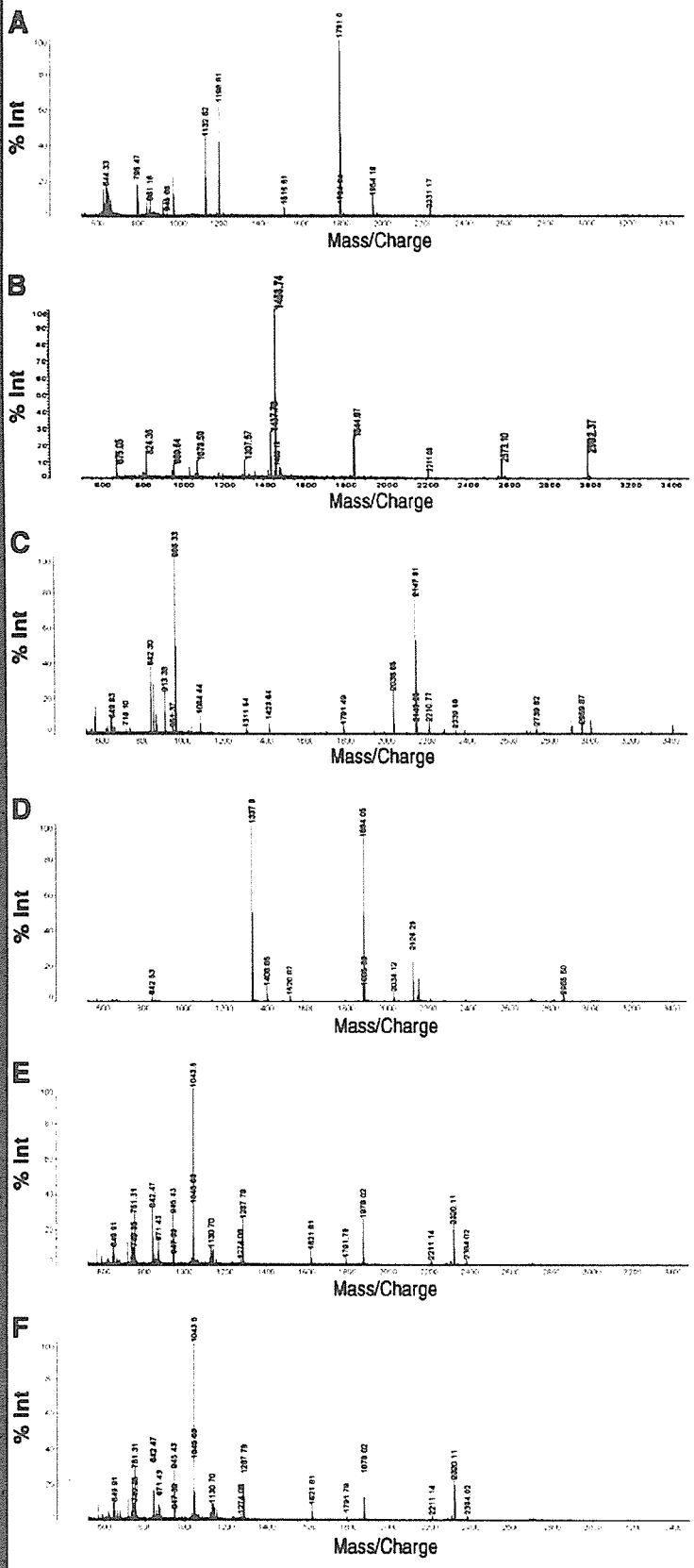

Fig. 2. Peptide mass fingerprinting (PMF) of *spots a–e*. *Spots a* (*B*), *b* (*C*), *c* (*D*), *d* (*E*), *e* (*F*) were picked, and, after trypsin digestion, matrix-assisted laser desorption ionization coupled to a time-of-flight mass spectrometer (MALDI-TOF-MS) analysis was performed. As a positive control, a β-actin spot (* in Fig. 1) was picked and analyzed (*A*).

Two-dimensional Western blotting. SYPRO Ruby-stained proteins on gels were resolubilized and transferred according to our previously reported method (23). Briefly, the stained gel was incubated in resolubilization buffer (0.2% wt/vol SDS, 0.3% wt/vol Tris, 0.7% wt/vol glycine) for 10 min and mounted onto a PVDF membrane in a semidry blotting apparatus (Bio-Rad Laboratories). Electrotransfer was carried out at 4 V/cm^2 for 1 h at room temperature using buffer containing 0.3% (wt/vol) Tris, 1.5% (wt/vol) glycine, 0.1% (wt/vol) SDS. The florescence images of the blotted PVDF membranes were scanned and recorded by FluorImager 595 (Amersham Biosciences). The PVDF membranes were further subjected to immunoblotting as in cases of 1-DE Western blotting.

Cell cycle analysis. Cells (5×10^5) were collected, washed with PBS, and fixed with 70% ice-cold ethanol for 4 h. After treatment with RNase A (100 μg/ml, Sigma) for 30 min at 37°C, DNA was stained with 50 μg/ml propidium iodide (Sigma). Cell cycle analysis was performed by FACScalibur (Becton-Dickinson, Mountain View, CA) using CELL Quest software according to the manufacturer's guidance.

Immunocytochemistry. Cells were fixed on slide glasses with a cytospin apparatus (Cytospin2; Shandon, Pittsburgh, PA) with further fixation with acetone-methanol solution (1:3). The immunostaining procedure was performed as described elsewhere (16) using anti-CLIC1 antibody (1:1,000 dilution) (24). The cells were observed by fluorescent microscopy with Normarsky differentiated interference contrast (Olympus Optical, Tokyo, Japan).

Statistical analysis. Student's *t*-test was used to determine statistical significance. A P value of <0.05 was considered significant.

RESULTS

2-DE protein expression profiles of human hematopoietic cells with or without insulin treatment. To identify novel downstream effectors in early phases of insulin-dependent signals in human hematopoietic cells, we performed the 2-DE-based differential protein expression analysis using human myeloblastic HL-60 cells. The cells which had been cultured in the absence of insulin for 3 days were treated with 5 μg/ml insulin or water. After 1 h, cell lysates were prepared according to the standard isoelectric focusing electrophoresis method described in MATERIALS AND METHODS. In this procedure, highly hydrophobic, urea-insoluble proteins were eliminated during the centrifugation step as precipitants, and only the supernatant fractions were used for 2-DE. In preliminary experiments, we used the immobilized pH gradient gel strip with a broad pH range (pH 3–10 nonlinear) for one-dimensional isoelectric focusing. Although more than 1,000 protein spots were visualized after SYPRO Ruby staining, PDQuest software-based analysis indicated that the spots having significant expression changes by insulin treatment were mainly located at pH 4–6 in the horizontal axis (data not shown). Thus we performed the following detailed analysis using the immobilized pH gradient gel strip with a narrower range (pH 4–7 linear) for finer resolution (Fig. 1). Over 600 protein spots were visualized by SYPRO Ruby staining. From these spots, we selected the candidates for the subsequent mass spectrometric analysis according to the following criteria. The basal expression level was higher than 5% of that of the largest β-actin spot, and the increase or decrease in the expression after insulin stimulation was greater than twofold or less than one-half, respectively. After statistical analysis of the multiple experiments (n = 3–6), five candidates were determined (Fig. 1). These spots were picked from the gel and, after trypsin digestions, MALDI-TOF-MS analysis was performed. Figure 2 shows the PMF of each spot, with a PMF of β-actin as a positive control. These data were further analyzed, being sent to the Mascot search server, and it was suggested that *spot a* was CLIC1, *spot b* was Rho-GDI-2, *spot c* was glutathione *S*-transferase-pi (GST-pi), and *spots d* and *e* were SRp20 (Fig. 2 and Table 1). The Mascot score of each search result was 175 (*spot a*), 80 (*spot b*), 98 (*spot c*), 100 (*spot d*), and 64 (*spot e*), indicating that the protein identifications by PMF were highly reliable (the data are summarized in Table 1). The results of the statistical analysis for the expression amounts of these spots are summarized in Table 2. Among these spots, Rho-GDI-2 (*spot b*) and GST-pi (*spot c*) have already been identified as downstream effectors of insulin. Rho-GDI-2 is reportedly released from the intracellular membrane fractions to the cytoplasm by insulin (19), and the expression of GST-pi markedly increases after insulin stimulation (6). Thus we focused our research on the evaluation of *spot a* and *spots d* and *e*.

To confirm the Mascot search results, we performed 2-DE western blotting by transferring SYPRO Ruby-stained 2-DE protein spots to PVDF membrane. As shown in Fig. 3*A*, most of the proteins were properly transferred to the membrane with a SYPRO Ruby pattern similar to that of the original gel. As shown in Fig. 3*B*, *spot a* was indeed recognized by anti-CLIC1

Table 2. *Ratios of spot intensities (insulin+/insulin−)*

Spot	Protein	Means ± SD	*P* Value
a	CLIC1	1.83±0.37	<0.01
b	Rho-GDI-2	2.03±0.43	<0.02
c	GST-pi	1.93±0.52	<0.05
d	SRp20	0.24±0.33	<0.01
e	SRp20	0.18±0.27	<0.005

Summarized results from 3–6 independent experiments are shown. Statistical analysis was performed by Student's *t*-test.

Table 1. *Protein identification by mass spectrometry analysis*

Spot	GenBank Acc. No.	Protein Name	Mr		pI		Mascot Score	Peptides		Sequence Coverage, %
			Theo, Da	O bs, kDa	Theo	Obs		Match	Total	
a	O00299	CLIC1	2,7248	29.0	5.09	5.16	175	10	11	47
b	P52566	Rho-GDI-2	2,3031	23.6	5.10	5.08	80	6	9	24
c	P09211	GST-pi	2,3438	22.9	5.44	5.67	98	6	8	48
d	P23152	SRp20	1.9546	21.2	11.64	6.13	100	9	11	43
e	P23152	SRp20	1.9546	20.5	11.64	6.38	100	9	11	43

Values of theoretical isoelectric points (pI) and molecular weights/masses (Mr) were obtained from Mascot search results. Theo, theoretical; Obs, observed; CLIC1, intracellular chloride ion channel; Rho-GDI-2, Rho-guanine nucleotide dissociation inhibitor 2; GST-pi, glutathione-*S*-transferase-pi; SRp20, a splicing factor. Calculations of experimental isoelectric point (pI) and molecular weight (Mr) were based on migration of the protein spot on 2-D gels using PDQuest.

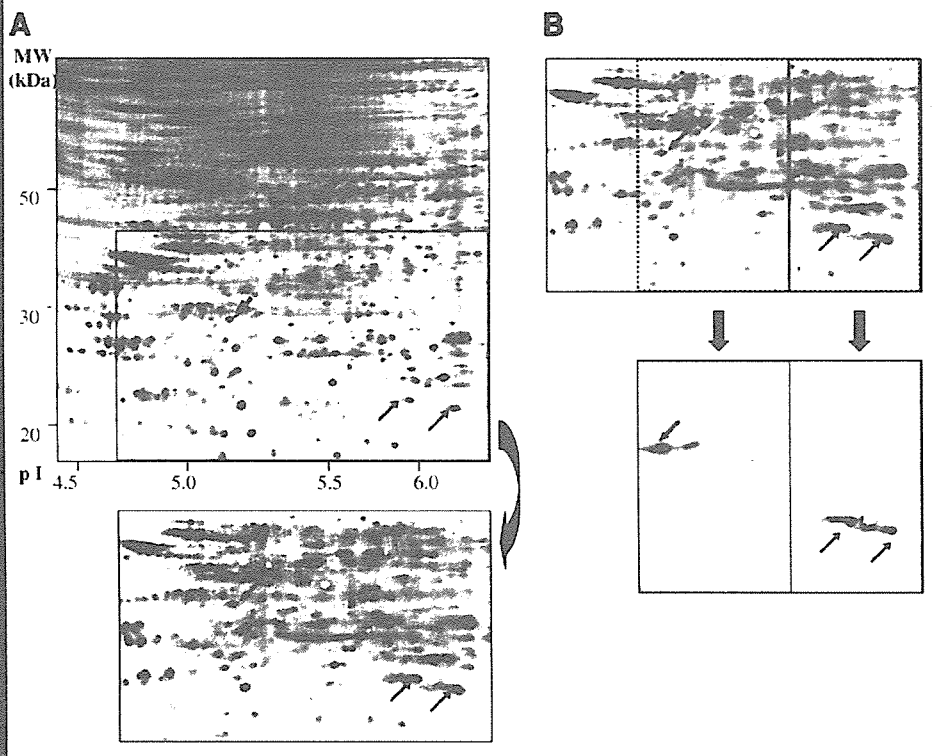

Fig. 3. 2-DE Western blotting. *A*: SYPRO Ruby-stained 2-DE gel, in which the lysate of buffer solution-treated cells were applied as in Fig. 1, *left*, was trimmed (*top*) and transferred onto a PVDF membrane (*bottom*). Transferred proteins were visualized by fluorescence image scanner. *B*: PVDF membrane was cut as indicated and blotted by anti-CLIC1 antiserum (*bottom left*) or anti-SRp20 antiserum (*bottom right*). Spots for CLIC1 and SRp20 are indicated with black arrows. Note that there is an extra spot on the anti-CLIC1-blotted membrane (indicated with white arrow).

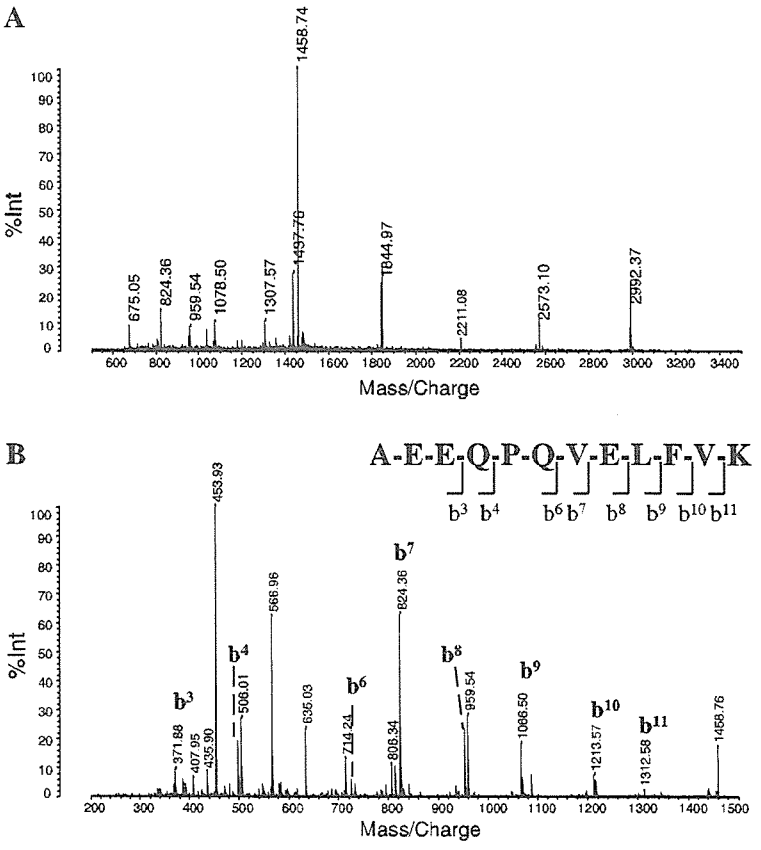

Fig. 4. Amino acid sequencing of NH_2-terminal peptide fragment of CLIC1. Parent ion at *m/z* 1,458.74 in Fig. 2*B* in insulin-treated cells was subjected to subsequent analysis using MS/MS mode of MALDI-TOF-MS (AXIMA-QIT). The mass data of b-series of the product ions were analyzed by the PepSeq program in ProteinLynx software. NH_2-terminal acetylated peptides of *N*-acetyl-AEE (*m/z* 372.14, b^3 ion), *N*-acetyl-AEEQ (*m/z* 500.20, b^4 ion), *N*-acetyl-AEEQPQ (*m/z* 725.30, b^6 ion), *N*-acetyl-AEEQPQV (*m/z* 824.38, b^7 ion), *N*-acetyl-AEEQPQVE (*m/z* 953.42, b^8 ion), *N*-acetyl-AEEQPQVEL (*m/z* 1,066.50, b^9 ion), *N*-acetyl-AEEQPQVELF (*m/z* 1,213.57, b^{10} ion), and *N*-acetyl-AEEQPQVELFV (*m/z* 1,312.64, b^{11} ion) were detected. Peptide mass fingerprinting (PMF; *A*) and MS/MS data of b-series (*B*) are shown. Similar analysis concerning control cells also demonstrated NH_2-terminal acetylation of CLIC1 (data not shown).

antibody and *spots d* and *e* were recognized by anti-SRp20 antibody. We also studied the possible modifications on these two proteins. As shown in Fig. 1*A*, the observed isoelectric point (pI) of CLIC1 was 5.16, which is similar to the Mascot information (the calculated pI was 5.09). Interestingly, there was an extra small spot with a higher pI value (Fig. 3*B*, white arrow). Indeed, we detected a doublet band in one-dimensional Western blotting, where the lysate prepared for 2-DE was mixed with an isovolume of 2× Laemmli's sample buffer and subjected to SDS-PAGE (data not shown and see Fig. 6*B*). Thus CLIC1 is expressed in at least two forms with different pI values in human hematopoietic cells, although the molecular basis for this difference was not elucidated. The MS digest analysis of *spot a* in the 2-DE profiles of both the insulin-treated and control cells demonstrated that the peptide fragment at mass-to-charge ratio (*m/z*) 1,458.74 in PMF of *spot a* represented the NH_2 terminus acetylated fragment acetyl-AEEQPQVELFVK, indicating that the first methionine was eliminated and the second alanine was N-acetylated. This finding was indeed confirmed by the amino acid sequencing at the *m/z* 1,458.74 fragment by the MS/MS mode of MALDI-TOF-MS, as shown in Fig. 4.

As for SRp20, the observed pI values of *spots d* and *e* were 6.13 and 6.38, respectively (Fig. 1 and Table 1), in contrast to the Mascot software information (the calculated pI was 11.64). This discrepancy may come from the modifications of SRp20. The MS digest analysis indicated that the SRp20 was phosphorylated at two sites, including Ser^{115} and Ser^{108}, from the existence of the peptide fragment ions of *m/z* 751.31 and *m/z* 945.43 (Fig. 5*A*). Mass value of *m/z* 751.31 is speculated amino acid sequences as $RRSPR_{(113-117)}$, $RSPRR_{(114-118)}$, or $SPRRR_{(115-119)}$ (Fig. 5*E*). As concerns *m/z* 945.43, MS digest suggests the amino acid sequence as $RRSPPPR_{(106-112)}$, $RSPPPRR_{(107-113)}$, or $SPPPRRR_{(108-114)}$. Phosphorylated peptide was confirmed by MALDI-TOF-MS in a seamless PSD mode (AXIMA-CFR) that detected the neutral loss of phosphate group. As shown in Fig. 5, *B* and *C*, phosphorylation-dependent neutral loss (−80 Da) and dehydration (−18 Da) were detected in the fragments at *m/z* 751.31 and *m/z* 945.43. Conversely, the MALDI-TOF-MS PSD spectrum of the control peptide ion gated at *m/z* 1,043.57 showed no significant neutral loss (Fig. 5*D*). Next, the amino acid sequences of *m/z* 751.31, *m/z* 945.43, and *m/z* 1,043.57 were examined by the same method as described above by using AXIMA-CFRplus. The amino acid sequences of *m/z* 751.31 could not be determined because the fragment ion was low intensity (data not shown). However, it is presumable that the Ser^{115} is phosphorylated. From the mass spectra of gated ion at *m/z* 945.43, the amino acid sequence was determined as $RRSPPPR_{(106-112)}$, and the position of phosphorylation was Ser^{108} (Fig. 6*A*). As a

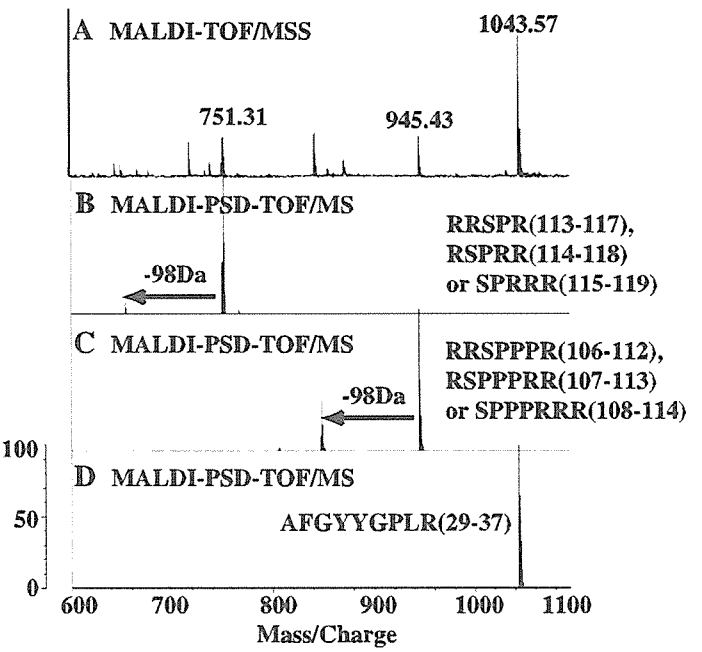

Fig. 5. Confirmation of SRp20 phosphorylation at specific serine residues. *A*: gated ions at *m/z* 751.31, 945.43, and 1,043.57 in Fig. 2*E* were subjected to analysis of neutral loss by MALDI-TOF-MS (AXIMA-CFR) in post-source decay (PSD) mode. The 98-Da loss of mass values was detected in gated ion at *m/z* 751.31 (*B*) and *m/z* 945.43 (*C*), but not in gated ion at *m/z* 1,043.57 (*D*) as a negative control. *E*: primary sequence of SRp20. *Phosphorylated amino acid.

E 1 MHRDSCPLDC KVYVGNLGNN GNKTELERAF GYYGPLRSVW VARNPPGFAF

m/z 1043.57

51 VEFEDPRDAA DAVRELDGRT LCGCRVRVEL SNGEKRSRNR GPPPSWGRRP

101 RDDYRRRS*PP PRRRS*PRRRS FSRSRSRSLS RDRRRERSLS RERNHKPSRS

m/z 945.43 *m/z* 751.31

151 FSRSRSRSRS NERK

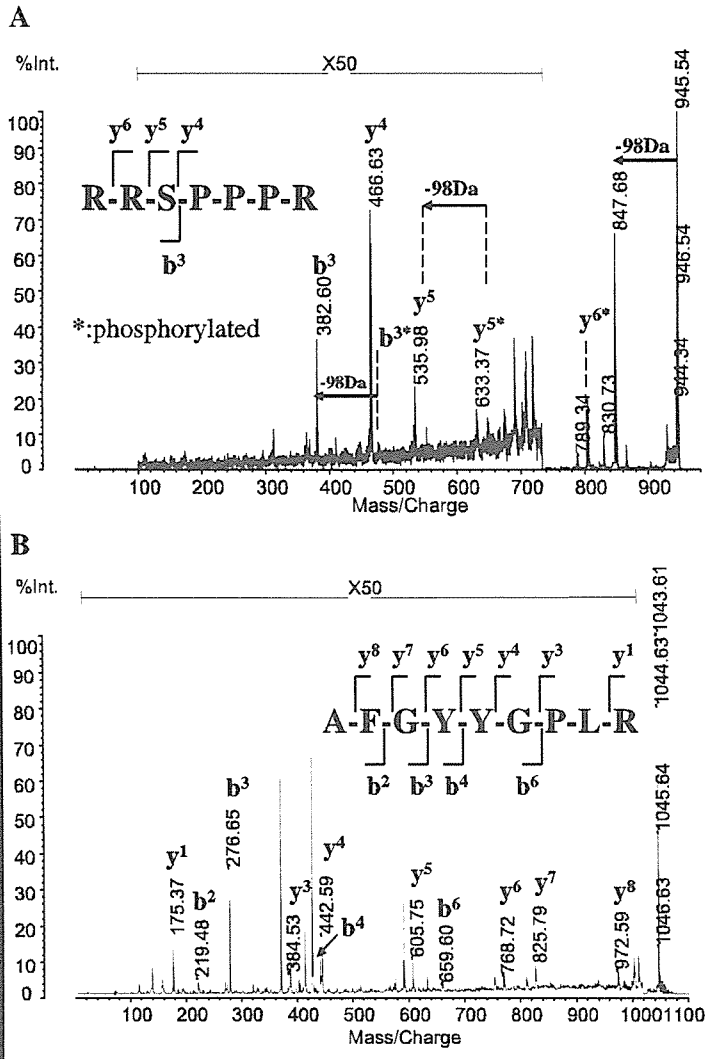

Fig. 6. Sequence analysis of gated ions at *m/z* 945.43 and 1,043.57 by MALDI-TOF-MS in PSD mode. *A*: gated ion at *m/z* 945.29 in Fig. 5*C* was subjected to subsequent analysis using PSD mode of MALDI-TOF-MS (AXIMA-CFRplus) *B*: three neutral loss ions (−98 Da) of *m/z* 480, 633, and 945 were detected. Gated ion at *m/z* 1,043.57 in Fig. 5*D* was subjected to the same analysis. Neutral loss ion (−98 Da) was not detected.

negative control, *m/z* 1,043.57 was subjected to analysis using PSD mode of AXIMA-CFRplus (Fig. 6*B*). The amino acid sequence was decided as AFGYYGPLR$_{(29-37)}$, which was not phosphorylated. These results indicated that Ser^{115} and Ser^{108} were phosphorylated in human hematopoietic cells (Fig. 5*E*). Thus the two phosphorylations of SRp20 may be responsible for the acidic shift of SRp20 in 2-DE.

Thus the 2-DE-based differential protein expression analysis identified CLIC1 and SRp20 as novel downstream effectors of insulin in human myeloblastic HL-60 cells.

1-DE study of CLIC1 and SRp20 expressions after insulin stimulations. It is known that there are occasionally discrepancies between the results of 2-DE and 1-DE. The difference in the protein solubilization capacities between the two systems is thought to be one of the reasons. During cell lysate preparation in 2-DE, highly hydrophobic proteins are prone to make precipitations and thus be eliminated from the lysates after centrifugation. Thus the protein expression changes in 2-DE-based proteome analysis not only means that the net protein expression changes but also the changes in protein solubilization. So we studied the expressions of CLIC1 and SRp20 after insulin stimulation by 1-DE Western blotting.

In contrast to the results of 2-DE, there was no significant difference in CLIC1 expression between insulin-treated and nontreated samples in 1-DE (Fig. 7*A*). Moreover, CLIC1 was detected as a single band, unlike the 2-DE results, where CLIC1 was detected as two spots. Interestingly, CLIC1 was detected as a doublet band, and the expression amounts of CLIC1 were indeed upregulated by insulin stimulation when the 2-DE lysates were treated by an isovolume of 2× Laemmli's buffer and subjected to 1-DE (Fig. 7*B*, *lane 2*). These findings strongly suggest that insulin treatment induced certain qualitative changes of CLICL1. Compared with 1-DE, the protein recovery rate in 2-DE was generally low: one-fourth the recovery as for CLICI (Fig. 7*B*, compare *lanes 1* and *3*) and one-eighth the recovery as for β-tubulin (Fig. 7*B*, compare *lanes 1* and *3*). However, the expression amounts of β-tubulin (Fig. 7*B*, compare *lanes 1* and *2*) and α-tubulin (data not shown) were not significantly changed by insulin treatment even in 2-DE lysates. By contrast, around a twofold increment in CLIC1 was reproducibly observed after insulin stimulation (Fig. 7, *B* and *C*, and data not shown). We then examined the possibility that the insulin-mediated increments in CLIC1 in 2-DE lysate were associated with the changes in its subcellular

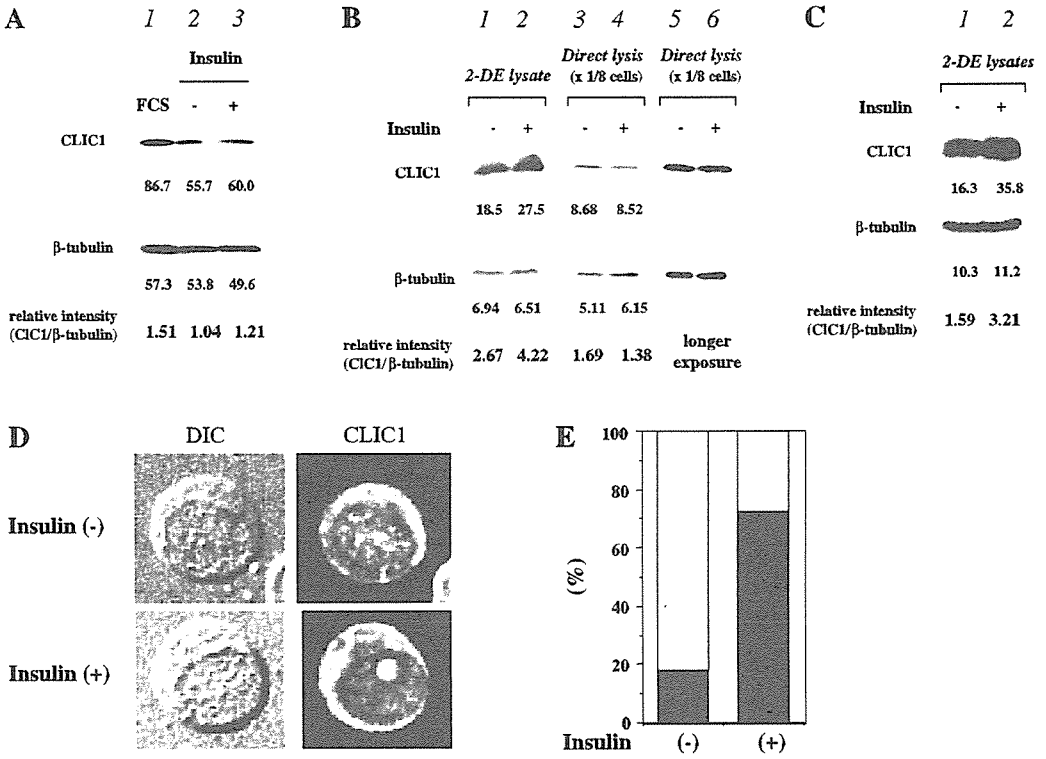

Fig. 7. 1-DE Western blotting of CLIC1. Cells that had been cultured with transferrin-supplemented serum-free medium for 3 days were stimulated by buffer solution (*lane 2*) or insulin (*lane 3*) and incubated for another 1 h at 37°C. *A*: cells were directly lysed with 1× Laemmli's sample buffer and subjected to 1-DE. Western blotting was performed using anti-CLIC1 antiserum. The lysate of the cells that had been cultured in the presence of FCS was also subjected to 1-DE (*lane 1*). Numeral under each band indicates intensity of the protein band. After the first antibody was stripped, the PVDF membrane was reblotted with anti-β-tubulin antibody. *B*: cell lysates prepared according to 2-DE protocol were mixed with isovolume of 2× Laemmli's sample buffer (*lanes 1* and *2*). One-eighth of the cells were directly lysed with 1× Laemmli's sample buffer and subjected to 1-DE (*lanes 3* and *4*). Longer exposure results of *lanes 3* and *4* are shown in *lanes 5* and *6*, respectively. *C*: results of independently performed experiment from *B* are shown. *D* and *E*: subcellular localization of CLIC1. *D*: insulin-treated or nontreated HL-60 cells were stained with anti-CLIC1 antibody. DIC, photograph with Normarsky differentiated interference contrast. *E*: percentages of cells with nuclear speckled staining pattern (filled bars) and cells with nucleoli-staining pattern (gray bars) are shown.

localization. As shown in Fig. 7, *D* and *E*, the nuclear localization pattern of CLIC1 was clearly changed by insulin treatment: CLIC1 was detected mainly as speckled forms in nuclear matrix in nontreated cells, whereas CLIC1 was located mainly at nucleoli in insulin-treated cells. Thus the changes in subnuclear localization may responsible for the expressional changes of CLIC1 in 2-DE.

Next, we studied the expression of SRp20 in 1-DE Western blotting. The SRp20 expression was actually reduced as in the case of 2-DE (Fig. 8*A*), indicating that the total amount of SRp20 was reduced by insulin treatment. To further investigate the molecular basis of insulin-mediated reduction in SRp20, the effects of the proteasome inhibitor MG-132 were examined. As shown in Fig. 8*B*, MG-132 inhibited the insulin-mediated reduction of SRp20 in a dose-dependent manner. MG-132 also blocked the degradation of cyclin D3 and enhanced the accumulation of cyclin D3 after insulin stimulation (Fig. 8*B*, *lane 5*). Interestingly, the recovery of SRp20 expres-

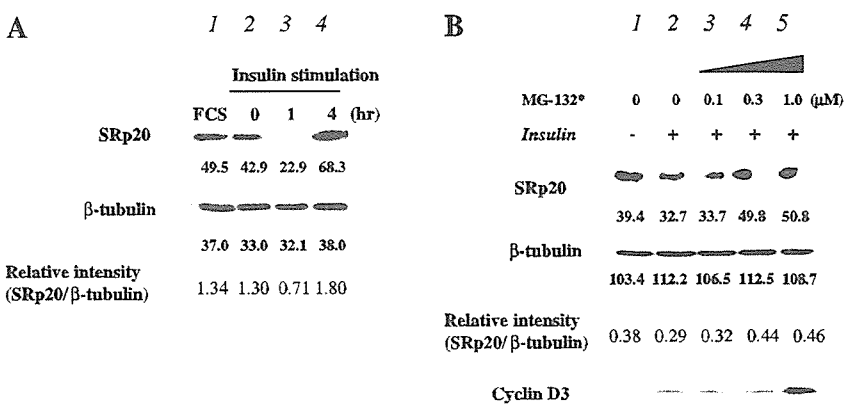

Fig. 8. 1-DE Western blotting of SRp20. Cells were cultured with transferrin-supplemented serum-free medium for 3 days. *A*: cells were then stimulated with insulin, and cell lysates were prepared at indicated times (*lanes 2–4*). Western blotting was performed using anti-SRp20 antiserum. The lysate of cells cultured in the presence of FCS was also subjected to 1-DE (*lane 1*). Numeral under each band indicates intensity of protein band. After the first antibody was stripped, PVDF membrane was reblotted with anti-β-tubulin antibody. *B*: DMSO or increasing doses of MG-132 were added 30 min before insulin stimulation. Cell lysates were prepared 1 h after stimulation and subjected to 1-DE. Western blotting was performed using anti-SRp20 antiserum. PVDF membrane was reblotted with anti-β-tubulin antibody and further with cyclin D3 antibody.

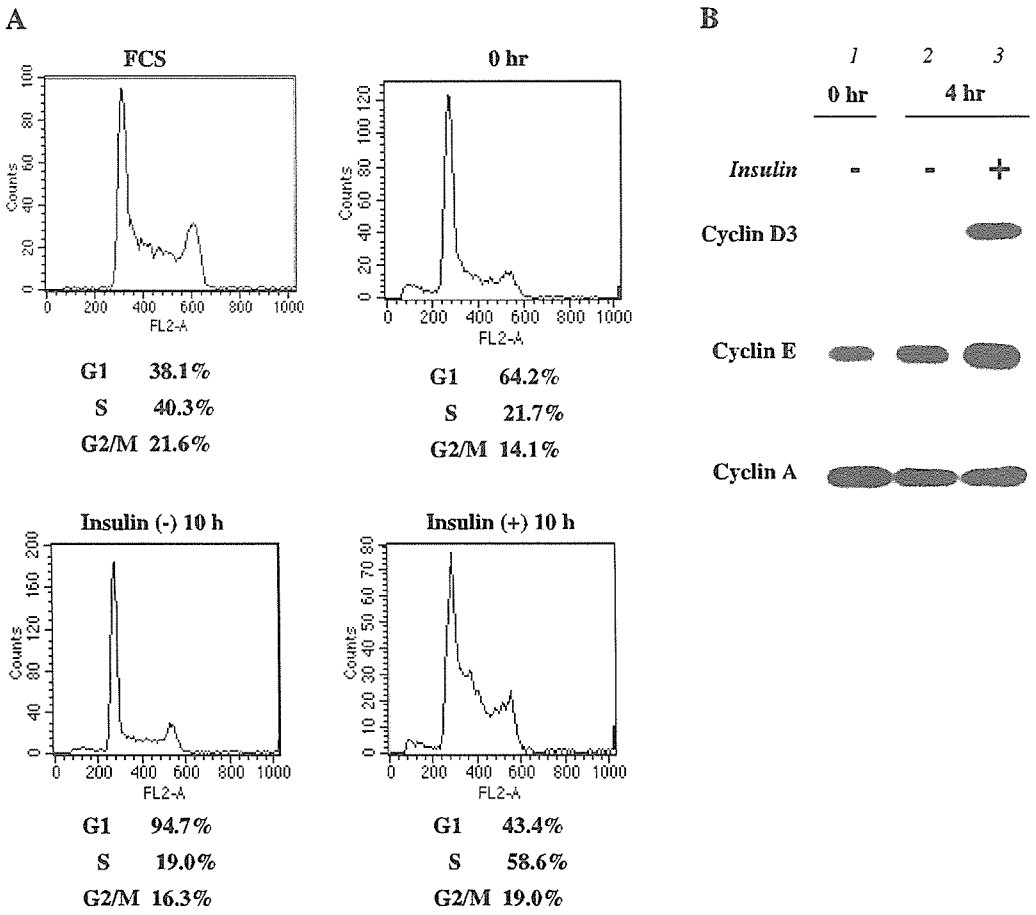

Fig. 9. Cell cycle analysis and expressions of cyclins. *A*: cells cultured with transferrin-supplemented serum-free medium for 3 days were stimulated with buffer solution (*bottom left*) or insulin (*bottom right*). After another 10-h incubation at 37°C. cells were fixed with 70% ethanol and subjected to DNA content assessment by fluorescence-activated cell sorting. Cells cultured in the presence of serum were also subjected to flow cytometric analysis (*top left*). *B*: cells cultured with transferrin-supplemented serum-free medium for 3 days were stimulated with buffer solution (*lane 2*) or insulin (*lane 3*). Cell lysates were prepared after another 4-h incubation. Western blotting was performed using anti-cyclin D3, followed by anti-cyclin E and anti-cyclin A reblotting.

sion was observed 4 h after stimulation (Fig. 8*A*, *lane 4*). Because serum stimulation activates SRp20 transcription and increases the protein expression of SRp20 as the cells enter into S-phase (9), the recovery in SRp2 expression would be associated with the cell cycling progression. As shown in Fig. 9, the insulin treatment significantly increased the S-phased population. Thus the recovery in SRp20 in later phases is associated with an enhanced S-entry.

Thus insulin treatment causes qualitative changes of CLIC1 that are associated with its subnuclear localization and the proteasome-dependent degradations of SRp20 as early as 1 h.

DISCUSSION

We identified CLIC1 and SRp20 as novel downstream effectors of insulin-dependent signals in human hematopoietic cells by using a 2-DE-based proteome analytic system.

A 2-DE-based proteome analysis has merit in managing a wide spectrum of protein expressions atone time. Moreover, it can illustrate the change in modifications and subcellular localization of the proteins besides the change in net amounts. As in the case of CLIC1, glyceraldehyde-3-phosphate dehydrogenase (GAPDH) expressions in 2-DE were upregulated by insulin stimulation, although no significant changes were detected in 1-DE (K. Saeki, unpublished observation). Because serum stimulation, which often induces similar protein expression changes as insulin stimulation, reportedly induces cytoplasmic transport of GAPDH (18), the upregulated expression of GAPDH in 2-DE may be associated with similar subcellular translocation.

Although CLIC1 functions as a chloride ion channel when localized to membranes (26), it is known that CLIC1 localizes principally to the cell nucleus in human hematopoietic cells (24). CLIC1 is structurally homologous to the GST superfamily of proteins with a redox-active site at the NH_2 terminus (5). It is suggested that CLICL1 activity is under the control of redox-active signaling molecules in vivo (5). In this sense, it is interesting that GST-pi is also a downstream effector of insulin as we showed (Fig. 1*A*, *spot c*) and reported elsewhere (6). It is known that hyperglycemia and, to a lesser extent, insulin resistance cause oxidative stress (15, 13). Insulin signaling might possibly contribute to the reduction of oxidative stresses by changing the expression patterns of CLICL1 and GST-pi. Further investigations are required to understand the molecular basis and biological relevance of insulin-induced changes in CLIC1 in the 2-DE system.

As for *spots d* and *e* of SRp20, we could not find any differences in PMFs. One interpretation is that distinct phosphorylations took place at their COOH-terminal SR domains. Because the SR domain is extremely rich in arginine residues, this domain should be degraded into pieces after trypsin digestion, and, as a result, the peptide fragment ions might be hardly detectable. In any case, the expressions of *spots d* and *e* were both decreased by insulin stimulation, and thus the precise determination of structural differences between the two spots would be a less important subject for an understanding of biological effects of insulin. As we showed, the insulin-induced reduction in SRp20 was inhibited by pretreatment of the cells by MG-132, a reversible proteasome inhibitor (Fig. 8*B*). Quite unexpectedly, lactacystin, an irreversible proteasome inhibitor, could not inhibit the reduction of SRp20, although it effectively enhanced an insulin-dependent accumulation of cyclin D3 (K. Saeki, unpublished observation), suggesting that there might be at least two different proteasome-dependent protein degradation systems with distinct lactacystin susceptibilities.

What is the impact of SRp20 reduction by insulin? SRp20 is a splicing factor involved in the regulation of alternative splicing of certain precursor RNA, including SRp20 itself. Its roles for embryogenesis have been shown: an inactivation of SRp20 gene in mice resulted in a failure to form blastocysts, and embryos died at morula stage (11). Although complete loss of SRp20 functions is toxic, its mild reduction may play roles in particular situations. It is reported that overexpression of ASF/SF2, an alternative splicing regulator that antagonizes the function of SRp20 (10), was detected in malignant ovarian tissues (4). A transient reduction of SRp20 by insulin might upregulate the activity of ASF/SF2 and thus trigger signals for cell proliferation. Further investigations are required to determine the in vivo significance of a transient reduction of SRp20 after insulin stimulation.

ACKNOWLEDGMENTS

We greatly thank Masaki Yamada and Tsutomu Nishine of Shimadzu Corporation for technical assistance with the amino acid sequence analysis performed using an MS/MS and PSD mode of MALDI-TOF-MS (AXIMA-QIT and AXIMA-CFRplus).

GRANTS

This work was supported, in part, by a grant for diabetes research (MF-4) from the Organization for Pharmaceutical Safety and Research (to Y. Kaburagi).

REFERENCES

1. **Araki E, Lipes MA, Patti ME, Bruning JC, Haag B III, Johnson RS, and Kahn CR.** Alternative pathway of insulin signalling in mice with targeted disruption of the IRS-1 gene. *Nature* 372: 186–190, 1994.
2. **Blommaart EF, Luiken JJ, Blommaart PJ, van Woerkom GM, and Meijer AJ.** Phosphorylation of ribosomal protein S6 is inhibitory for autophagy in isolated rat hepatocytes. *J Biol Chem* 270: 2320–2326, 1995.
3. **Edvardsson U, Alexandersson M, Brockenhuus von Lowenhielm H., Nystrom AC, Ljung B, Nilsson F, and Dahllof B.** A proteome analysis of livers from obese (ob/ob) mice treated with the peroxisome proliferator WY14,643. *Electrophoresis* 20: 935–942, 1999.
4. **Fischer DC, Noack K, Runnebaum IB, Watermann DO, Kieback DG, Stamm S, and Stickeler E.** Expression of splicing factors in human ovarian cancer. *Oncol Rep* 11: 1085–1090, 2004.
5. **Harrop SJ, DeMaere MZ, Fairlie WD, Reztsova T, Valenzuela SM, Mazzanti M, Tonini R, Qiu MR, Jankova L, Warton K, Bauskin AR, Wu WM, Pankhurst S, Campbell TJ, Breit SN, and Curmi PM.** Crystal structure of a soluble form of the intracellular chloride ion channel CLIC1 (NCC27) at 1.4-A resolution. *J Biol Chem* 276: 44993–5000, 2001.
6. **Hatayama I, Yamada Y, Tanaka K, Ichihara A, and Sato K.** Induction of glutathione S-transferase P-form in primary cultured rat hepatocytes by epidermal growth factor and insulin. *Jpn J Cancer Res* 82: 807–814, 1991.
7. **Jaleel A and Nair KS.** Identification of multiple proteins whose synthetic rates are enhanced by high amino acid levels in rat hepatocytes. *Am J Physiol Endocrinol Metab* 286: E950–E957, 2004.
8. **Joshi RL, Lamothe B, Cordonnier N, Mesbah K, Monthioux E, Jami J, and Bucchini D.** Targeted disruption of the insulin receptor gene in the mouse results in neonatal lethality. *EMBO J* 15: 1542–1547, 1996.
9. **Jumaa H, Guenet JL, and Nielsen P.** Regulated expression and RNA processing of transcripts from the Srp20 splicing factor gene during the cell cycle. *Mol Cell Biol* 17: 3116–3124, 1997.
10. **Jumaa H and Nielsen PJ.** The splicing factor SRp20 modifies splicing of its own mRNA and ASF/SF2 antagonizes this regulation. *EMBO J* 16: 5077–5085, 1997.
11. **Jumaa H, Wei G, and Nielsen PJ.** Blastocyst formation is blocked in mouse embryos lacking the splicing factor SRp20. *Curr Biol* 9: 899–902, 1999.
12. **Kaburagi Y, Yamauchi T, Yamamoto-Honda R, Ueki K, Tobe K, Akanuma Y, Yazaki Y, and Kadowaki T.** The mechanism of insulin-induced signal transduction mediated by the insulin receptor substrate family. *Endocr J* 46, *Suppl*: S25–S34, 1999.
13. **King GL and Loeken MR.** Hyperglycemia-induced oxidative stress in diabetic complications. *Histochem Cell Biol* 122: 333–338, 2004.
14. **Liu JP, Baker J, Perkins AS, Robertson EJ, and Efstratiadis A.** Mice carrying null mutations of the genes encoding insulin-like growth factor 1 (Igf-1) and type 1 IGF receptor (Igf1r). *Cell* 75: 59–72, 1993.
15. **Robertson RP.** Chronic oxidative stress as a central mechanism for glucose toxicity in pancreatic islet beta cells in diabetes. *J Biol Chem* 279: 42351–42354, 2004.
16. **Saeki K, Hong Z, Nakatsu M, Yoshimori T, Kabeya Y, Yamamoto A, Kaburagi Y, and Yuo A.** Insulin-dependent signaling regulates azurophil granule-selective macroautophagy in human myeloblastic cells. *J Leukoc Biol* 74: 1108–1116, 2003.
17. **Sasaoka T and Kobayashi M.** The functional significance of Shc in insulin signaling as a substrate of the insulin receptor. *Endocr J* 47: 373–381, 2000.
18. **Schmitz HD.** Reversible nuclear translocation of glyceraldehyde-3-phosphate dehydrogenase upon serum depletion. *Eur J Cell Biol* 80: 419–427, 2001.
19. **Shisheva A, Buxton J, and Czech MP.** Differential intracellular localizations of GDP dissociation inhibitor isoforms. Insulin-dependent redistribution of GDP dissociation inhibitor-2 in 3T3-L1 adipocytes. *J Biol Chem* 269: 23865–32868, 1994.
20. **Sun XJ, Rothenberg P, Kahn CR, Backer JM, Araki E, Wilden PA, Cahill DA, Goldstein BJ, and White MF.** Structure of the insulin receptor substrate IRS-1 defines a unique signal transduction protein. *Nature* 352: 73–77, 1991.
21. **Sun XJ, Wang LM, Zhang Y, Yenush L, Myers MG Jr, Glasheen E, Lane WS, Pierce JH, and White MF.** Role of IRS-2 in insulin and cytokine signalling. *Nature* 377: 173–177, 1995.
22. **Tobe K, Tamemoto H, Yamauchi T, Aizawa S, Yazaki Y, and Kadowaki T.** Identification of a 190-kDa protein as a novel substrate for the insulin receptor kinase functionally similar to insulin receptor substrate-1. *J Biol Chem* 270: 5698–5701, 1995.
23. **Toda T, Sugimoto M, Omori A, Matsuzaki T, Furuichi Y, and Kimura N.** Proteomic analysis of Epstein-Barr virus-transformed human B-lymphoblastoid cell lines before and after immortalization. *Electrophoresis* 21: 1814–1822, 2000.
24. **Valentinis B, Romano G, Peruzzi F, Morrione A, Prisco M, Soddu S, Cristofanelli B, Sacchi A, and Baserga R.** Growth and differentiation signals by the insulin-like growth factor 1 receptor in hemopoietic cells are mediated through different pathways. *J Biol Chem* 274: 12423–12430, 1999.
25. **Valenzuela SM, Martin DK, Por SB, Robbins JM, Warton K, Bootcov MR, Schofield PR, Campbell TJ, and Breit SN.** Molecular cloning and expression of a chloride ion channel of cell nuclei. *J Biol Chem* 272: 12575–12582, 1997.
26. **Warton K, Tonini R, Fairlie WD, Matthews JM, Valenzuela SM, Qiu MR, Wu WM, Pankhurst S, Bauskin AR, Harrop SJ, Campbell TJ, Curmi PM, Breit SN, and Mazzanti M.** Recombinant CLIC1 (NCC27) assembles in lipid bilayers via a pH-dependent two-state process to form chloride ion channels with identical characteristics to those observed in Chinese hamster ovary cells expressing CLIC1. *J Biol Chem* 277: 26003–26011, 2002.

ダイヤモンドライクカーボンおよびフッ素添加ダイヤモンドライクカーボンの医用応用

～医療応用目的のナノメディカルデバイス研究開発の基盤作りについて～

長谷部光泉，上條亜紀，堀田篤，髙橋孝喜，鈴木哲也

表面技術 第56巻 第12号(2005)別刷